

**MODULAR PEBBLE BED REACTOR PROJECT  
UNIVERSITY RESEARCH CONSORTIUM  
ANNUAL REPORT**

**INEEL/EXT-2000-01034  
MIT-ANP-PR-075**

**July 2000**

**MIT COLLABORATORS**

**Andrew C. Kadak  
Ronald G. Ballinger  
Michael J. Driscoll  
Sidney Yip  
David Gordon Wilson  
Hee Cheon No  
Jing Wang  
Heather MacLean  
Tamara Galen  
Chunyun Wang  
Julian Lebenhaft  
Tieliang Zhai**

**INEEL COLLABORATORS**

**David A. Petti  
William K. Terry  
Hans D. Gougar  
Abderrafi M. Ougouag  
Chang H. Oh  
Richard L. Moore  
Gregory K. Miller  
John T. Maki  
Galen R. Smolik  
Dominic J. Varacalle**



# MODULAR PEBBLE BED REACTOR

## ABSTRACT

This project is developing a fundamental conceptual design for a gas-cooled, modular, pebble bed reactor. Key technology areas associated with this design are being investigated which intend to address issues concerning fuel performance, safety, core neutronics and proliferation resistance, economics and waste disposal. Research has been initiated in the following areas:

- Improved fuel particle performance
- Reactor physics
- Economics
- Proliferation resistance
- Power conversion system modeling
- Safety analysis
- Regulatory and licensing strategy

Recent accomplishments include:

- Developed four conceptual models for fuel particle failures that are currently being evaluated by a series of ABAQUS analyses. Analytical fits to the results are being performed over a range of important parameters using statistical/factorial tools. The fits will be used in a Monte Carlo fuel performance code, which is under development.
- A fracture mechanics approach has been used to develop a failure probability model for the fuel particle, which has resulted in significant improvement over earlier models.
- Investigation of fuel particle physio-chemical behavior has been initiated which includes the development of a fission gas release model, particle temperature distributions, internal particle pressure, migration of fission products, and chemical attack of fuel particle layers.
- A balance of plant, steady-state thermal hydraulics model has been developed to represent all major components of a MPBR. Component models are being refined to accurately reflect transient performance.
- A comparison between air and helium for use in the energy-conversion cycle of the MPBR has been completed and formed the basis of a master's degree thesis.
- Safety issues associated with air ingress are being evaluated.
- Post shutdown, reactor heat removal characteristics are being evaluated by the Heating-7 code.
- PEBBED, a fast deterministic neutronic code package suitable for numerous repetitive calculations has been developed. Use of the code has focused on scoping studies for MPBR design features and proliferation issues. Publication of an archival journal article covering this work is being prepared.
- Detailed gas reactor physics calculations have also been performed with the MCNP and VSOP codes. Furthermore, studies on the proliferation resistance of the MPBR fuel cycle has been initiated using these code
- Issues identified during the MPBR research has resulted in a NERI proposal dealing with turbo-machinery design being approved for funding beginning in FY01. Two other NERI proposals, dealing with the development of a burnup "meter" and modularization techniques, were also funded in which the MIT team will be a participant.
- A South African MPBR fuel testing proposal is pending (\$7.0M over nine years).



## CONTENTS

Abstract .....	ii
1.0 Project Description.....	1
2.0 Gas Reactor Fuel Performance.....	2
2.1 Background .....	3
2.2 Stress Model Development and Approach.....	4
2.3 Statistical Techniques .....	11
2.3.1 One Dimensional Results .....	12
2.3.2 Two Dimensional Results .....	15
2.4 Mechanical Modeling .....	16
2.5 Fuel Particle Thermal Model .....	19
2.6 Fission Product Behavior Experimental Program .....	20
3.0 Reactor Physics and Neutronics .....	22
3.1 Neutronics Analysis .....	22
3.1.1 Core Physics Background .....	22
3.1.2 Description of the Model .....	23
3.1.3 Results .....	27
3.2 Reactor Physics .....	37
3.2.1 HTR-10 Physics Benchmark.....	38
3.2.2 MCNP4B/VSOP94 Model of PBMR .....	41
3.2.3 Nonproliferation.....	44
4.0 Safety and Thermal Hydraulics .....	47
4.1 Power Conversion System Development .....	47
4.1.1 Plant Description .....	48
4.1.2 Power Conversion System Model Development .....	49
4.1.3 Working Fluid Comparison .....	54
4.2 Safety Analysis .....	56
5.0 Other Activities .....	61
5.1 Economics .....	61
5.2 Regulatory Licensing Strategy .....	61
6.0 Conclusions.....	62
References .....	63

## 1. Project Description

The Modular Pebble Bed Reactor (MPBR) is an advanced reactor concept that can meet the energy and environmental needs of future generations as defined under DOE's Generation IV initiative. Preliminary research has concluded that this technology has an excellent opportunity to satisfy the safety, economic, proliferation and waste disposal concerns that face all nuclear electric generating technologies. Our work directly supports INEEL's mission as co-lead NE laboratory. Our work in collaboration with the Massachusetts Institute of Technology (MIT) is focused on developing, benchmarking, and applying core design tools in the areas of neutronics, thermal hydraulics, fuel performance and safety analysis. This strategy will allow INEEL to address the important issues that face the MPBR and to have a complete integrated reactor core design capability for the MPBR. In this report we provide a description of progress made in the past year. The work capitalizes on INEEL's historic strength in fuel development and testing (including extensive experience with light water reactor fuel, ATR-type fuel, and New-Production-Reactor particle fuel). The project also builds on the strong capabilities at INEEL and MIT for reactor core neutronics and thermal hydraulic design, as well as nuclear safety analysis. The DOE has begun funding the development of a "4<sup>th</sup> generation" reactor with NERI funds and will try to budget significant line items within the next 5 years. If we are to compete for further nuclear energy development R&D, we need to demonstrate capability to design and build advanced reactors. The Modular Pebble Bed Reactor (MPBR) is an advanced reactor concept that can meet the energy and environmental needs of future generations.

During the current year, six MIT student researchers were involved, five of whom were supported by INEEL funds. Five MIT faculty supervised the students along with two senior research scientists. In addition, about 10 INEEL staff worked part time on different parts of the project. Below are the three major areas of research and the associated researchers:

Table 1-1. Research Demographics for the MBPR Project. (Leads are in Bold)

Research Area	Students	MIT Faculty and Staff	INEEL Staff
Fuel Performance	Jing Wang Heather MacLean (not supported)	Ron Ballinger Sidney Yip	David Petti John Maki Dominic Varacalle Greg Miller
Thermal Hydraulics and Safety	Tamara Galen Chunyun Wang Tieliang Zhai	Ron Ballinger Andrew C. Kadak David Gordon Wilson Walter Kato Hee Cheon No	David Petti Chang Oh Richard Moore Galen Smolik
Core Neutronics and Physics	Julian Lebenhaft	Andrew C. Kadak Michael J. Driscoll	William Terry Hans D. Gougar Abderrafi M. Ougouag

## 2. Gas Reactor Fuel Performance

As has been described in earlier reports, the fuel performance effort has been divided into two major areas. The first area is focused on the fuel itself and the associated buffer layer. In this region we address modeling of phenomena associated with the fuel including all chemical aspects, fission product production and release, fuel swelling and/or densification, buffer densification and the calculation of internal pressure. Work in this area includes an experimental program to evaluate the migration and release of silver through the SiC layer as well as the interaction of palladium with the SiC layer and it's potential effect on layer failure. The second area of focus deals with the mechanical aspects of fuel performance and includes the performance of the pyrocarbon and SiC layers. This area focuses on a complete analysis of the mechanical aspects of fuel performance including the evolution of the behavior of the layers. Work in this area also is tasked with the development of a fuel failure model.

While the two areas of fuel performance are being treated separately, this is only for convenience. Unlike the LWR case, where there is a significant interaction between the fuel and the cladding, in the case of the MPBR the presence of the low density buffer layer surrounding the fuel kernel mechanically isolates the fuel from the pressure retaining layers (inner PyC, SiC, and outer PyC). Thus, the primary interactions between the two regions are associated with the fission gas pressure, the migration and release of silver, and the chemical interaction of the fission products with the SiC layer. The results of the effort in the two areas will be combined to produce an integrated fuel performance model. Figure 21 shows a schematic of the integration of the overall model.

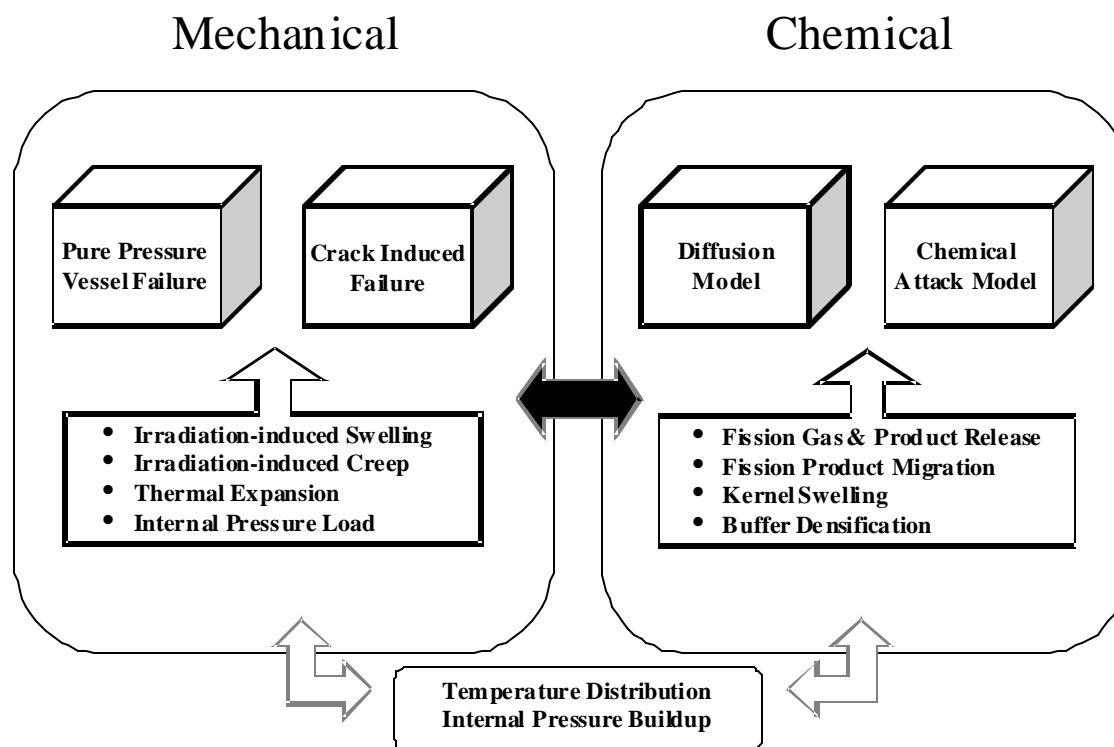


Figure 2-1. Schematic of the fuel performance modeling effort integration.

## 2.1 Background

The success of gas reactors depends upon the safety and high quality of the coated particle fuel. To aid in the evaluation of such coated particle fuels, we are developing an integrated *mechanistic* fuel performance model that will allow optimization of fuel particle design and offer a connection between processing, properties, and ultimate fuel performance.

Compared to light water reactor and breeder reactor fuel forms, the behavior of coated particle fuel is inherently more multidimensional. Moreover, modeling of fuel behavior is made more difficult because of statistical variations in fuel physical dimensions and/or component properties, from particle to particle due to the nature of the fabrication process. There has historically been some debate in the gas reactor community about whether a mechanistic model development effort for this fuel would be successful. Previous attempts to model this fuel form have attacked different pieces of the problem. Simplified one-dimension models exist to describe the structural response of the fuel particle. Models or correlations exist to describe the fission product behavior in the fuel, though the database is not complete owing to the changes in fuel design that have occurred over the last 25 years. Significant effort has gone into modeling the statistical nature of fuel particles. However, under pressure to perform over one million simulations with the computing power available in the 1970s and 1980s, the structural response of the particle was simplified to improve the speed of calculation.

No publicly available integrated mechanistic model for particle fuel exists as an accurate tool for nuclear design. The advent of powerful personal computers and the tremendous advancements in fundamental modeling of materials science processes now enable more accurate simulations of particle fuel behavior to be performed. We are developing and will verify a first-principles-based mechanistic, integrated, thermal-mechanical-chemical-irradiation performance model for particle fuel, which has the proper dimensionality yet, captures the statistical nature of the fuel. Furthermore, the verified fuel performance model would allow advanced particle fuel to be designed with greater confidence for the gas reactor and other particle fuel applications.

Fuel development for this fuel form has included the traditional in-reactor experiments followed by postirradiation examination. Thus, there is a modest experimental database on the irradiation behavior of particle fuel. However, the *integral* behavior of the coating system under irradiation is complicated, and previous attempts to characterize it have been only partially successful. While many of the variables critical to fuel performance are known, it is not clear that all the important phenomena have been identified. The irradiation behavior of coated particle fuel over the past three decades has been mixed. For example, the irradiation performance of German particle fuel has been very good, whereas for nominally the same processing parameters, U.S. gas reactor particle fuel performance has been much worse. There have not been significant changes in the US in-pile fuel performance over the last three decades (based on data from References 1, 2, 3, 4, 5). The measured Kr-85m release-to-birth ratio (R/B) for all US experiments at the end of irradiation and for Ft. St. Vrain range between  $10^{-5}$  to  $10^{-4}$  at reactor level fluences. (This corresponds to 1-2% failure.) By comparison, R/B values obtained for German fuel under similar conditions are on the order of  $10^{-7}$  to  $10^{-6}$ . Unfortunately, the reasons for the historically poorer US performance relative to German fuel has been the subject of extensive debate but has never been definitively established. Clearly, a mechanistic integrated fuel performance model is needed. We are working on both the structural aspects and the physio-chemical aspects of a fuel performance model. Here we summarize recent highlights.

## 2.2 Stress Model Development and Approach

Symmetric one-dimensional models have historically been developed for gas reactor particles. The results of recent US irradiations indicate that asymmetric phenomena such as cracking and debonding are also important. A photomicrograph illustrating these effects is shown in Figure 2-2. Thus, we have developed four structural models of the TRISO-coated fuel particle using the ABAQUS finite element program:

- a traditional three layer coating system (IPyC/SiC/OPyC),
- a four layer coating system (Buffer/IPyC/SiC/OPyC),
- a cracked three layer model which has an initial crack in the IPyC and
- a debonded three layer model which has an initial debonding site between the IPyC and SiC

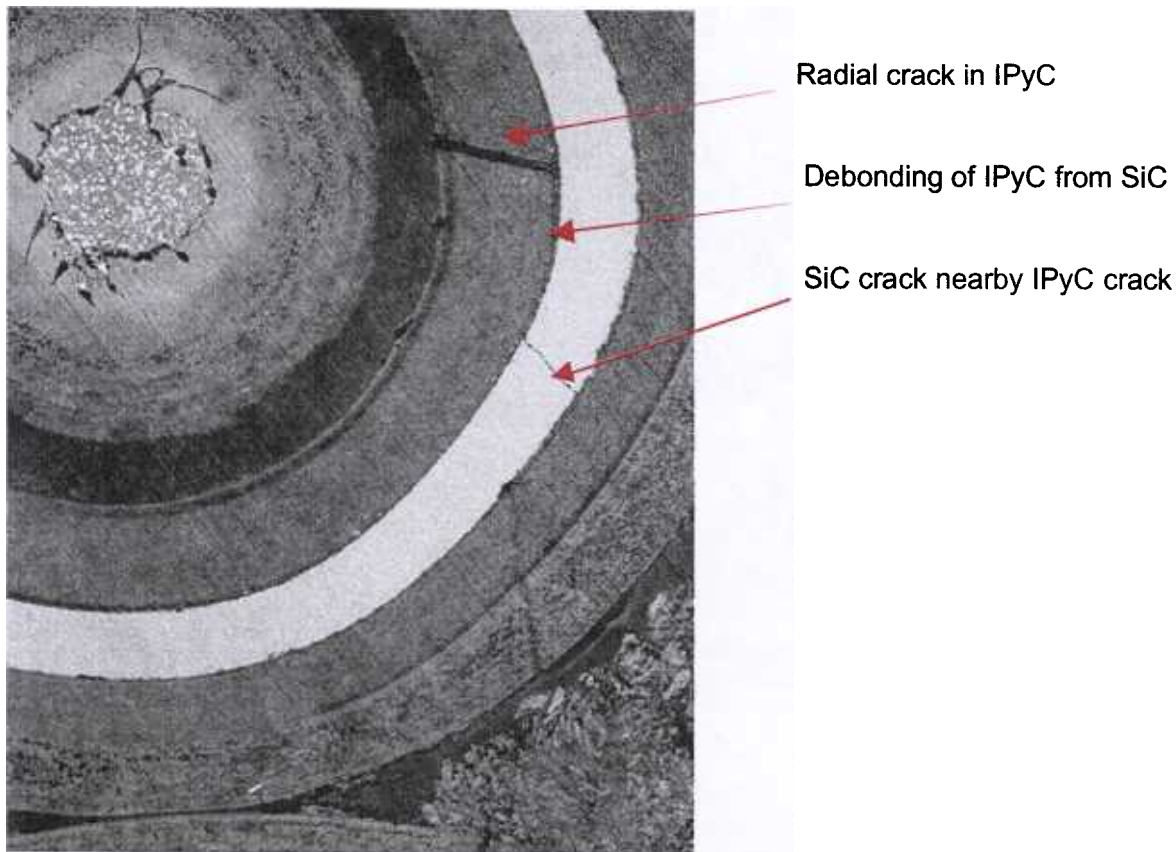


Figure 2-2. Photomicrograph of a failed U.S. New Production Reactor fuel particle.

ABAQUS models for the three-layer and cracked three-layer model are shown in Figure 2-3. Our long-term goal is to use these models (or some subset of them) to determine the influence of properties (e.g. layer thicknesses, densities, and anisotropy) and irradiation (temperature, burnup, fluence) on the stress in the system in each of these models. Performing a systematic evaluation for each model will allow the construction of a multidimensional stress response surface as a function of all the important variables. This may require on the order of 1000 calculations using ABAQUS although we are examining more powerful statistical techniques that would reduce the number of calculations required. We will then use statistical techniques to



develop a simple yet accurate fit to the important variables that can be used in Monte Carlo simulations of large numbers of particles.

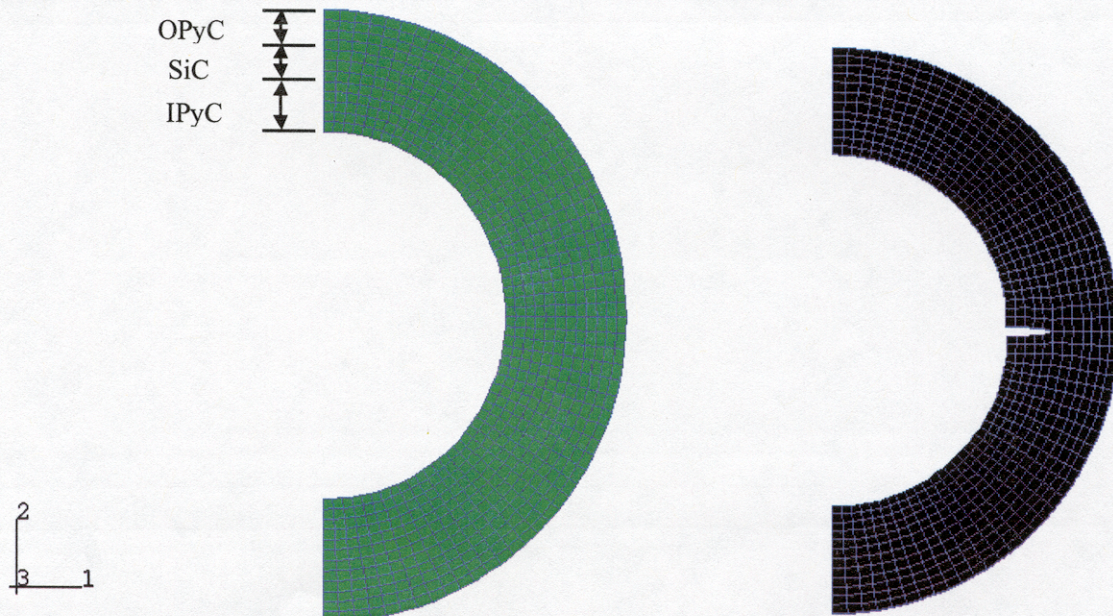


Figure 2-3. ABAQUS Models for the standard three layer and cracked three layer particles.

The basic behavior modeled in the three layer standard model is shown schematically in Figure 2-4. The IPyC and OPyC layers both shrink and creep during irradiation of the particle, while the SiC exhibits only elastic response (i.e., creep and swelling in the silicon carbide is negligible relative to that in the pyrocarbons). A portion of the fission gas pressure is transmitted through the IPyC layer to the SiC. This pressure continually increases as irradiation of the particle progresses, thereby contributing to a tensile hoop stress in the SiC layer. Countering the effect of the pressure load is the shrinkage of the IPyC during irradiation, which pulls inward on the SiC.

Due to anisotropy in the PyC shrinkage behavior, different strain rate histories evolve in the radial and tangential directions. The shrinkage in the radial direction reverses to swelling at moderate fluence levels, whereas shrinkage in the tangential direction continues to high fluence levels. These irradiation-induced strain rates are also functions of the degree of anisotropy as measured by the Bacon Anisotropy Factor (BAF) and the density of the pyrocarbon material. [A BAF of 1.0 corresponds to perfectly isotropic material and a BAF of infinity is completely anisotropic.] As with the IPyC, the OPyC shrinks, causing it to push inward on the SiC. An ambient external pressure may also be applied to the OPyC, depending on reactor conditions.

Figure 2-5 plots the tangential stress in a standard particle based on a 2-D ABAQUS calculation. As indicated in the figure, the SiC remains in compression largely because of the PyC shrinkage. During irradiation, the IPyC shrinks pulling on the SiC and the OPyC shrinks pushing on the SiC from the outside.



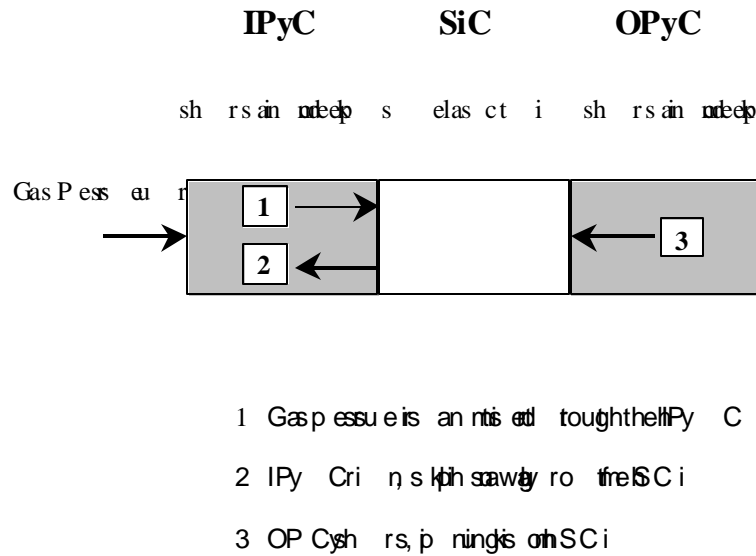


Figure 2-4. Behavior of TRISO coating during irradiation.

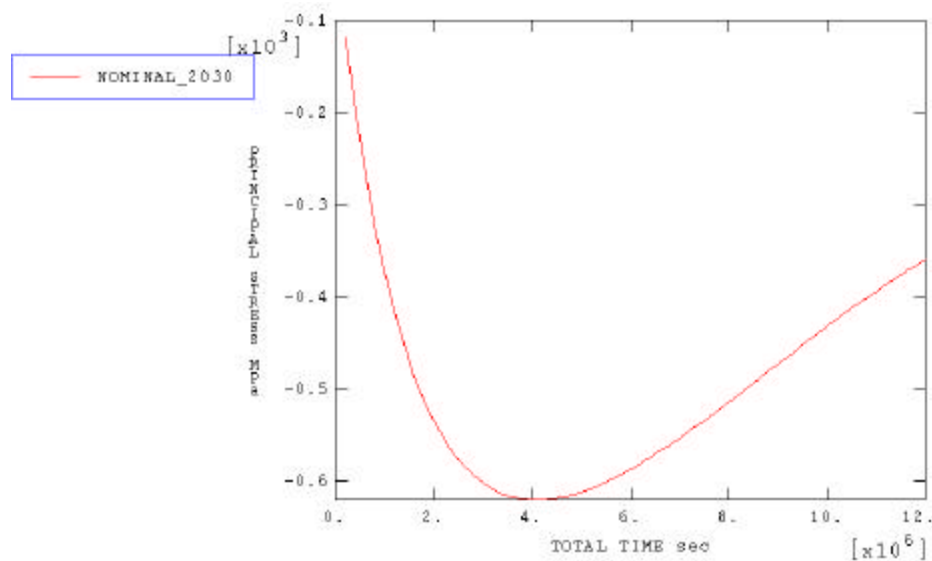


Figure 2-5. SiC tangential stress for a standard particle.

By comparison, the stress behavior in the SiC with a cracked IPyC is quite different. As shown in Figure 2-6, the crack leads to a tensile stress in the SiC with a magnitude on the order of 320 MPa. This large stress in the SiC near the crack in the PyC greatly changes the stress picture of the particle and increases the probability of SiC failure.

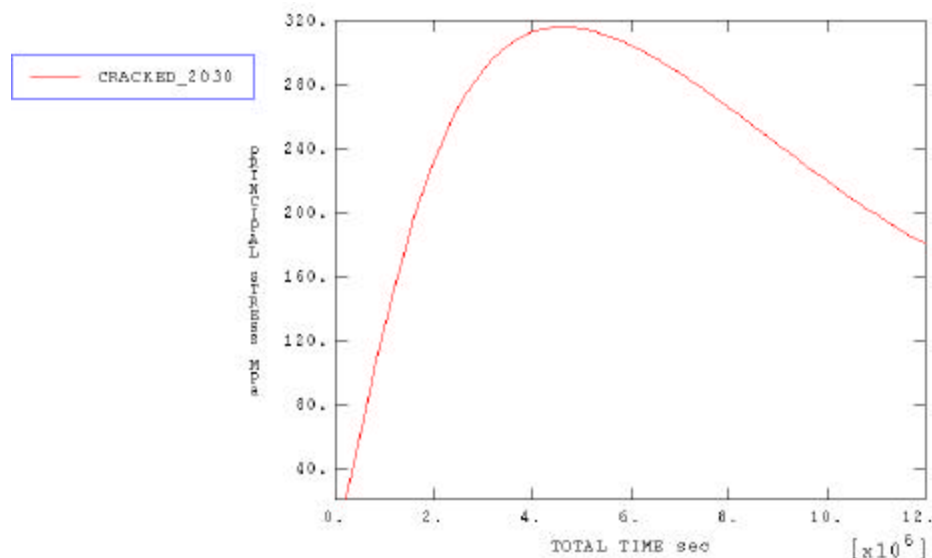


Figure 2-6. Principal stress in the SiC for a particle with cracked IPyC.

There is debate in the gas reactor community over the behavior of the pyrocarbon layers under irradiation. The level of failure during irradiation, the role of anisotropy on the resulting stress in the particle, the degree of IPyC/SiC debonding, and the strength of the IPyC are all issues with large uncertainties. All of these effects contribute to our incomplete understanding of the behavior of the IPyC under irradiation and its prominent role in the failure of the NP-MHTGR fuel particles. As a result, one of the recent developments has been to update our ABAQUS model to include more comprehensive material property correlations for the PyC and SiC layers based on a recent reassessment of the database by GA.<sup>6</sup> The correlations have a more complete description of the shrinkage and swelling of PyC as a function of density, temperature and fluence. In addition, the reassessment of the database has identified a greater functional dependency on other structural properties of SiC and PyC. All of these improvements are now in our ABAQUS models. Some recent results are shown below.

Figures 2-7 and 2-8 are plots of the dimensional change of PyC in both the radial and tangential directions as a function of fast neutron fluence and the degree of anisotropy. The more anisotropic the material (larger BAF) the greater the dimensional changes in both directions. In Figures 2-9 and 2-10, the effect of irradiation temperature on the dimensional change is shown. The results show that the shrinkage and swelling behavior of the PyC is greater at higher temperature. At a temperature of 700°C, the dimensional changes are less than at higher temperature. This is important because in an MPBR core, only a small fraction of the fuel is at the highest temperature. Thus, the role of PyC shrinkage and swelling is expected to be less at lower temperature. Also shown in the figures are data taken from irradiation experiments. The overall database is sketchy. There are no data below  $0.7 \times 10^{25} \text{ n/m}^2$ . The shapes of the curves are based on current understanding of graphite behavior under irradiation but the actual values are artifacts of the curve fit. Data also exist at high fluence ( $6 \times 10^{25} \text{ n/m}^2$ ) which were needed for the large gas reactor like Ft. St. Vrain. The validity of the fits at high fluence is open to question but since the MPBR design fluence is below  $3.7 \times 10^{25} \text{ n/m}^2$  the fits should be adequate for our needs. Because of the incomplete nature of the database, we are using a very broad range for anisotropy in the stress analysis (BAF from 1.0 to 1.33.). This range is much broader than is found in current manufacturing of fuel in an attempt to bracket the effect of anisotropy on particle behavior.



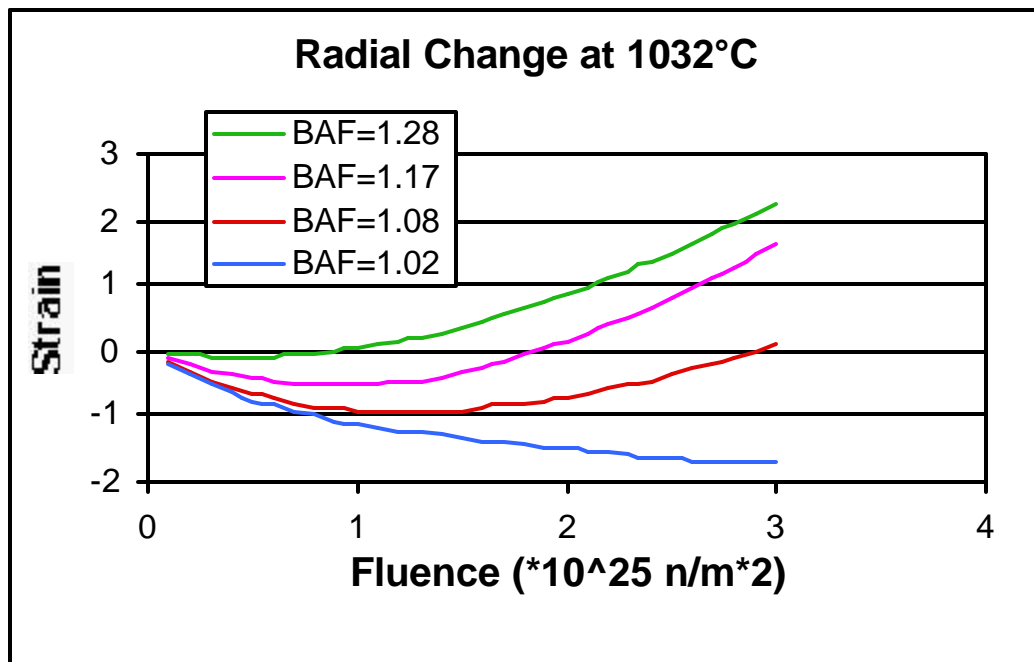


Figure 2-7. Radial change in PyC as a function of anisotropy (BAF) and fluence.

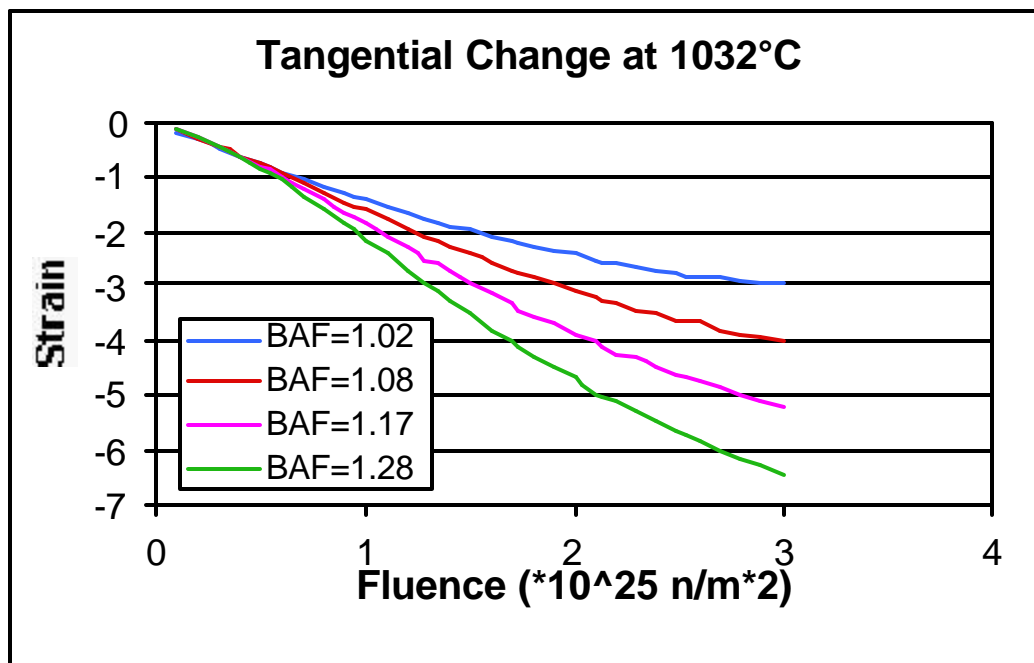


Figure 2-8. Tangential change in PyC as a function of anisotropy (BAF) and fluence.

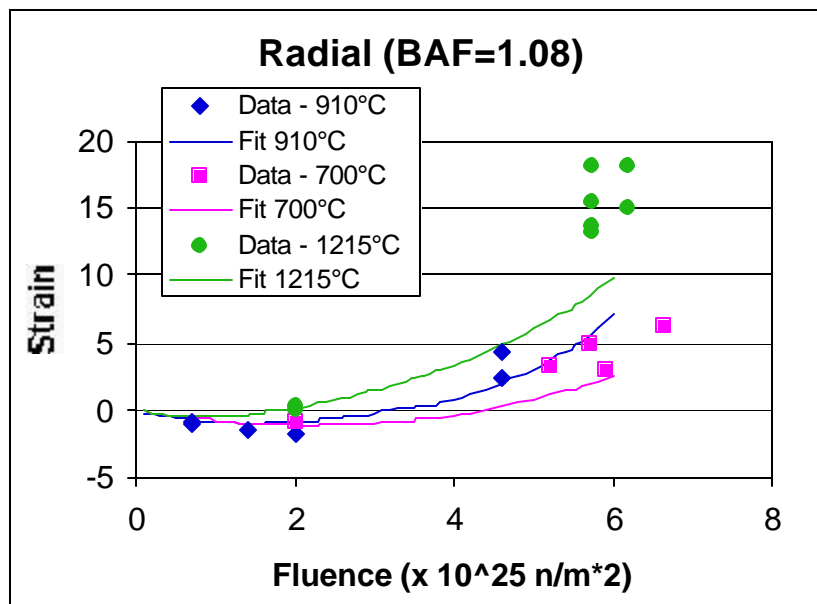


Figure 2-9. Radial change in PyC as a function of temperature and fluence.

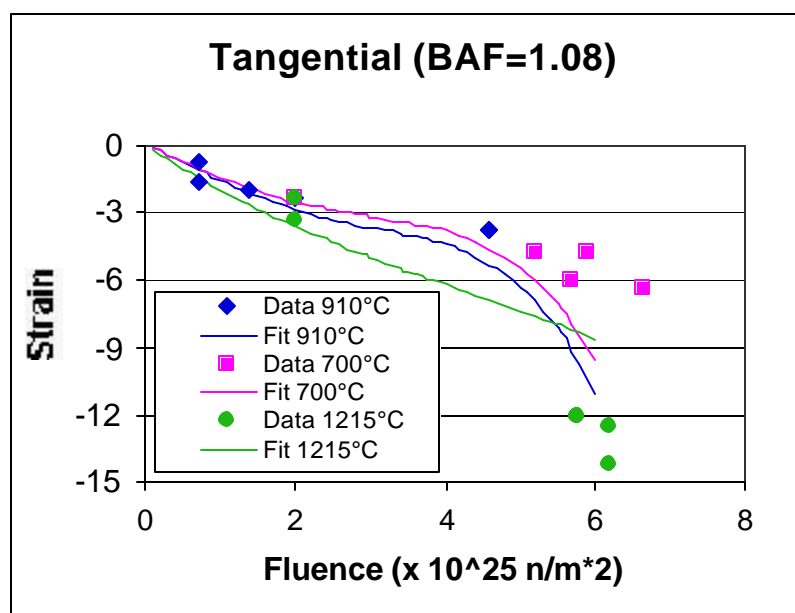


Figure 2-10. Tangential change in PyC as a function of temperature and fluence.

We have evaluated the effect of IPyC anisotropy on the stress in the SiC and IPyC layers using the three-layer standard model and the three-layer cracked model. We have performed ABAQUS calculations for BAFs ranging from 1 to 1.33, corresponding to the range in the NP-MHTGR fuel IPyC specification. (Note that for NP-MHTGR fuel particles, the measured BAFs ranged from 1.045 to 1.071, with a mean of 1.058.) For the standard particle, the irradiation-induced shrinkage puts the IPyC layer into tension. As shown in Figure 2-11, the IPyC stress is very sensitive to the BAF. The stress in the IPyC increases by about 50% as the BAF is changed from 1 to 1.33. Since the IPyC is believed to fail in a probabilistic manner according to Weibull theory, this increase in stress results in a large increase in the probability of failure based on traditional estimates of the Weibull strength of IPyC. The failure probability increases

from 40% at a BAF of 1.0 to near 100% at a BAF of 1.33. Thus, the more anisotropic the IPyC, the greater its propensity to fail via cracking. This agrees qualitatively with irradiation data of particles.

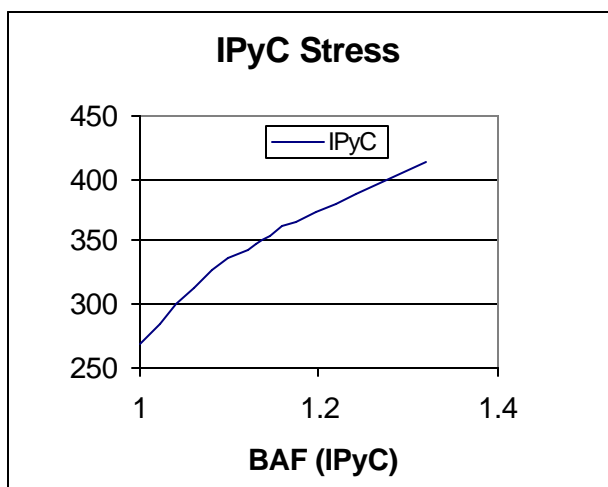


Figure 2-11. IPyC Stress as a function of BAF for standard three-layer model.

The recent data re-assessment on PyC behavior also has a new formulation for Weibull strength that is a very strong function of BAF. The results would suggest that as the BAF increases and the stress in the IPyC increases, the strength increases disproportionately such that the overall failure probability decreases as shown in Figure 2-12. This result is somewhat surprising and perhaps counterintuitive. Closer examination of this new strength formulation is currently underway in light of these results.

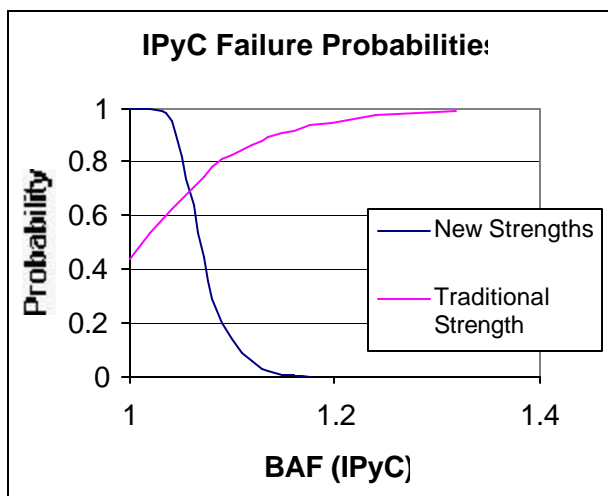


Figure 2-12. Probability of IPyC failure using traditional and new strength formulations.

For the same conditions, the SiC is put into heavy compression in the tangential directions early during irradiation and slight tension in the radial direction. A plot of the peak radial stress in the SiC as a function of BAF in the standard model is shown in Figure 2-13. In this case, the overall effect of changing the IPyC BAF on the stress in the SiC is small in the standard three-layer model. By comparison, in an initially cracked particle, the behavior is quite different. The increase in anisotropy increases the stress in the SiC near the crack quite dramatically, as

shown in Figure 2-13. As the BAF increases from 1 to 1.33, the stress in the SiC near the crack in the IPyC increases by 220%! (Failure of the SiC in this case requires a fracture mechanics approach, which has not yet been performed.) These results suggest that the BAF is a very sensitive parameter that could result in cracking of the IPyC, which could then accelerate failure of the SiC. We continue to perform calculations using the cracked and debonded models to understand their influence on particle integrity. Beyond that, our future work is focused on performing the systematic ABAQUS calculations for the four models discussed above and developing the statistical fits for the response surface.

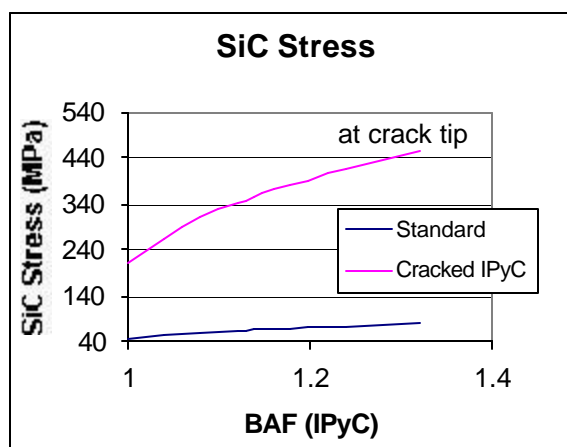


Figure 2-13. SiC stress as a function of BAF for standard and cracked IPyC three layer models.

## 2.3 Statistical Techniques

The finite element modeling presented in the previous section provides the most accurate solution to the stress in coated particle fuel. It incorporates all of the important phenomena at the proper level of dimensionality. Unfortunately, such a model is too cumbersome and computationally intensive for use in the proposed fuel performance model where over one million simulations must be performed as a part of a Monte Carlo analysis. Therefore, the approach that is proposed is to perform a number of detailed finite element calculations over a range of all the important input variables. Based on the finite-element results, factorial design methods and multi-variable statistical fits will be used to develop a fast running algorithm for use in the fuel performance model. Our judgment is that the results of the finite element run matrix will allow us to adequately characterize the range of expected behavior. Box-type statistical design techniques will be used to determine the proper set of finite element calculations, and state-of-the-art statistical analysis techniques will be used to determine the algorithm.

The Box-type statistical design of experiment (SDE) methodology<sup>7</sup> is an efficient means of determining broad-based factor effects on measured attributes. This methodology statistically delineates the impact of each input variable on the output across all combinations of other input and allows a quantitative understanding of the main effects and the possible interactions between the effects. An example of this type of factorial design approach is illustrated below.

In the case of three input variables studied at two levels (+1 and -1) for each variable, the full factorial design is shown in Table 2-1. The full factorial would require eight combinations to evaluate the impact of all three variables and all of their interactions (i.e., for variables A, B and C, the interactions are AB, AC, BC, ABC). If only experiments 1 through 4 were analyzed, this

would be considered a 1/2 fractional factorial experiment. Highly fractionalized analysis is to be avoided since it introduces significant error into the analysis. Such techniques are quite powerful for the case of many variables where interactions are not always apparent.

Table 2-1. Factor Level Combination for 2\*\*3 Factorial Experiment

		Factors/Input		
		A	B	C
Experiment 1	Levels	-1	-1	-1
Experiment 2	Levels	+1	-1	-1
Experiment 3	Levels	-1	+1	-1
Experiment 4	Levels	+1	+1	-1
Experiment 5	Levels	-1	-1	+1
Experiment 6	Levels	+1	-1	+1
Experiment 7	Levels	-1	+1	+1
Experiment 8	Levels	+1	+1	+1

### 2.3.1 One Dimensional Results

We have assessed the feasibility of such an approach using the results from a simple one-dimensional stress analysis of the particle. Analytical experiments using the SDE methodology were conducted to determine the feasibility of using regression analysis to replicate the results of the 1-D stress solution for the particle. The primary attribute of interest was the stress in the SiC layer. For the case presented here, the SDE design constituted a 2-level factorial response surface. (A higher level factorial design can be used depending on the problem of interest.) Two levels of each variable were established to provide a band around the nominal settings in order to demonstrate the capabilities of the technique at a variety of processing conditions.

The following fifteen parameters were investigated in the analytical studies:

- kernel diameter
- buffer thickness
- inner pyrolytic carbon (i.e. IPyC) thickness
- silicon carbide thickness
- outer pyrolytic carbon (i.e. OPyC) thickness
- end-of-life burnup
- irradiation temperature
- U<sup>235</sup> enrichment
- reactor pressure
- buffer mean density
- kernel mean density
- kernel theoretical density
- initial density of the inner PyC
- initial density of the outer PyC,
- fast fluence at the end of irradiation

High and low levels for each factor are listed in Table 2-2. Based on the box-type statistical design methodology and the 15 input variables, 209 different stress calculations were performed. Once the analytical calculations were conducted, the data were analyzed with the Design-Expert program.<sup>8</sup>

Effects analysis was first conducted for the stress in the SiC layer. Regression analysis of the results was performed based on linear, quadratic and cubic fits to the input variables. ANOVA (i.e. analysis of variance) analysis was then conducted to determine the adequacy of each of the three models. The results indicate that a linear fit was very good negating the need for higher order fits. Figure 2-14 illustrates the perturbation plot for stress showing the effect of each parameter on the SiC stress.

Table 2-2. SDE Design for Fuel Code

Factor	Units	Low Actual	High Actual
KERNDIA	microns	175.00	215.00
BUFFTHK	microns	80.00	120.00
IPYCTHK	microns	43.00	63.00
SICTHK	microns	25.00	45.00
OPYCTHK	microns	33.00	53.00
EOLBUP	%	60.00	80.00
TEMPIRR	K	1273.00	1673.00
U235ENR	%	90.00	96.00
PAMB	MPa	5.40	7.40
BUFFD	g/cm <sup>3</sup>	0.90	1.00
KERND	g/cm <sup>3</sup>	10.40	10.60
KERNT	g/cm <sup>3</sup>	11.00	11.06
IPYCD	g/cm <sup>3</sup>	1.81	2.02
PYCD	g/cm <sup>3</sup>	1.77	1.98
EOLFLU	10 <sup>21</sup> n/cm2	2.50	3.50

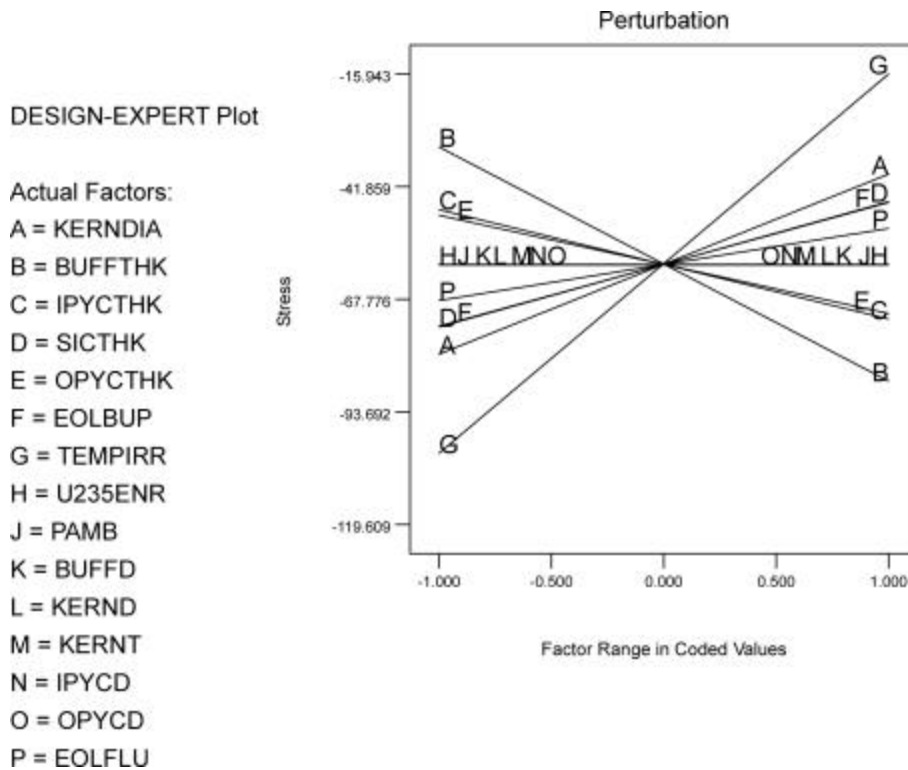


Figure 2-14. Perturbation plot for stress.

As shown in this example, irradiation temperature (49.5%) contributes most significantly to the stress on the particle, while kernel diameter (11.1%), and buffer thickness (18.8%) exhibit secondary influences. IPyC thickness (4.3%), silicon carbide thickness (5.6%), OPyC thickness (3.5%), end-of-life burnup (5.2%), and fast fluence at the end of irradiation (1.8%) have minor influence on the stress. The remaining parameters ( $U^{235}$  enrichment, reactor system pressure,

buffer mean density, kernel mean density, kernel theoretical density, measured density of the inner PyC, measured density of the outer PyC) have less than 0.1% influence on the stress.

The equation below illustrates the regression equation for the stress based on the linear model. This equation defines the input parameter-attribute relationship. Noted that the predicted attributes should not be extrapolated past the levels (ranges) of the parameters shown in Table 2-2.

$$\text{STRESS} = -562.33 + 1.02 \cdot \text{KERNDIA} - 1.40 \cdot \text{BUFFTHK} - 1.23 \cdot \text{IPYCTHK} + 1.82 \cdot \text{SICTHK} - 1.11 \cdot \text{OPYCTHK} + 1.40 \cdot \text{EOLBUP} + 0.23 \cdot \text{TEMPIRR} + 19.02 \cdot \text{EOLFLU}$$

Figure 2-15 illustrates the response surface plots of the stress as a function of buffer thickness and irradiation temperature. In this figure, all other parameters are held at their nominal values. The stress in the SiC layer decreases with lower irradiation temperature (because of less gas release and less gas pressure for a given number of moles) and higher buffer thickness (because of greater void volume available for gas release). Based on the effects analysis, the input parameters that lead to the greatest compressive stress in the SiC are: kernel diameter 175 microns, buffer thickness 120 microns, IPyC thickness 63 microns, silicon carbide thickness 25 microns, OPyC thickness 53 microns, end-of-life burnup 60%, irradiation temperature 1273K, and fast fluence at EOL  $2.5 \times 10^{21}$  n/cm<sup>2</sup>. The remaining input did not have a significant effect on the stress. Thus, nominal values were used for input in the point analysis, which predicts a stress of -220 MPa in the SiC under these conditions. This agrees very well with the value from the one-dimensional stress analysis.

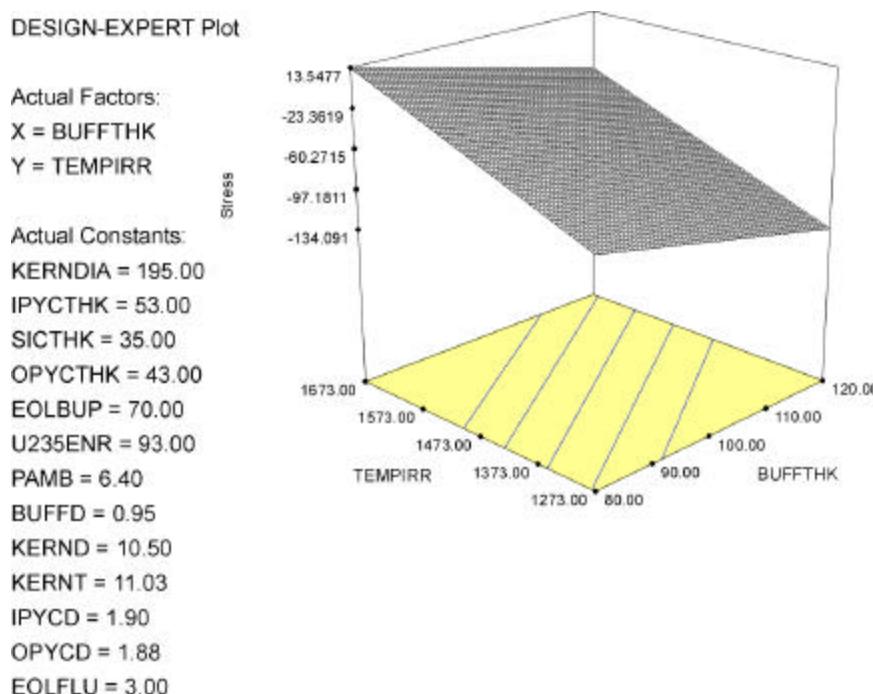


Figure 2-15. Response surface plot.

### 2.3.2 Two Dimensional Results

We have also performed similar statistical box type analysis using 2-D ABAQUS results for the standard three-layer model and for the cracked three-layer model. The following parameters in Table 2-3 and their corresponding ranges were used in the evaluations. These parameters and ranges are based on engineering judgement based on past gas reactor work. Using these parameters, a five-parameter, three-level factorial matrix was constructed. Calculations were performed for both the standard and cracked models. In each case, 243 2D ABAQUS calculations were performed. In each case, the SiC stress was the output variable that was correlation with the five input parameters in Table 2-3.

Table 2-3. Parameters and Ranges from 2-D 5 Parameter 3 Level Factorial Calculations

KEY PARAMETERS	Low	Medium	High
SiC Thickness (um)	30	40	50
IPyC Thickness (um)	30	40	50
IPyC Anisotropy (BAF)	1	1.16	1.33
IPyC Density (g/cc)	1.8	1.9	2
OPyC Thickness (um)	33	43	53

The results for the standard model, shown in Figure 2-16, indicate that an excellent statistical fit has been obtained. It is also interesting to note that the IPyC thickness and its anisotropy (BAF) has the greatest influence on the predicted behavior in a standard particle. (We note that the NPR particles had unusually thick IPyC -- 53 microns.)

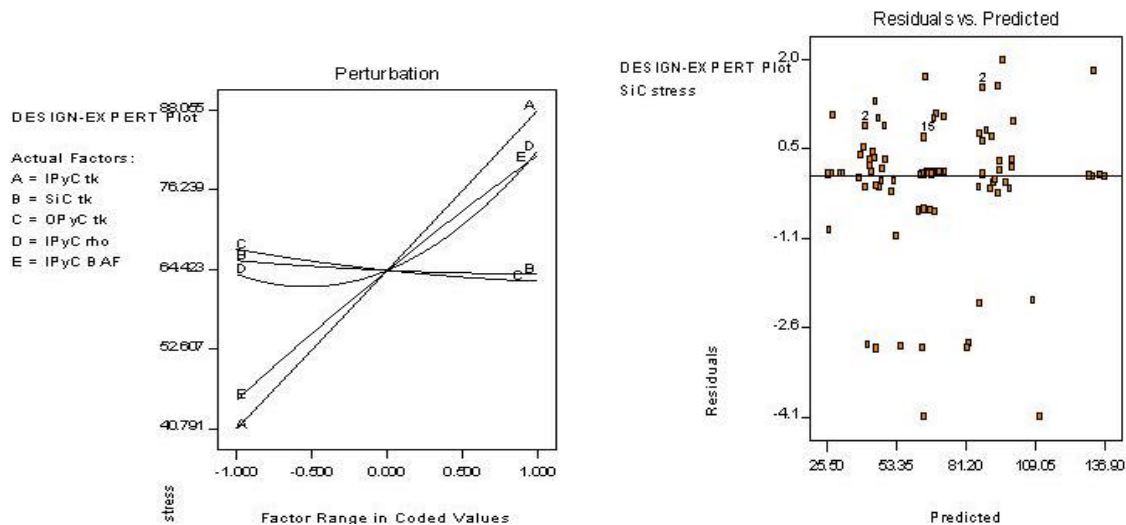


Figure 2-16. Statistical results from 5 parameter, 3 level factorial for the standard particle.

The results of the cracked model are shown in Figure 2-17. The statistical fit is quite good but not as good as in the case of the standard particle, largely because the stress analysis of the cracked particle is non-linear. The most important parameters are the IPyC density, IPyC anisotropy (BAF) and the IPyC thickness. The IPyC density is important because of its relationship to the IPyC creep coefficient. As the density of the IPyC increases above 1.9 g/cc, the creep coefficient decreases resulting in greater stresses in the IPyC and SiC.



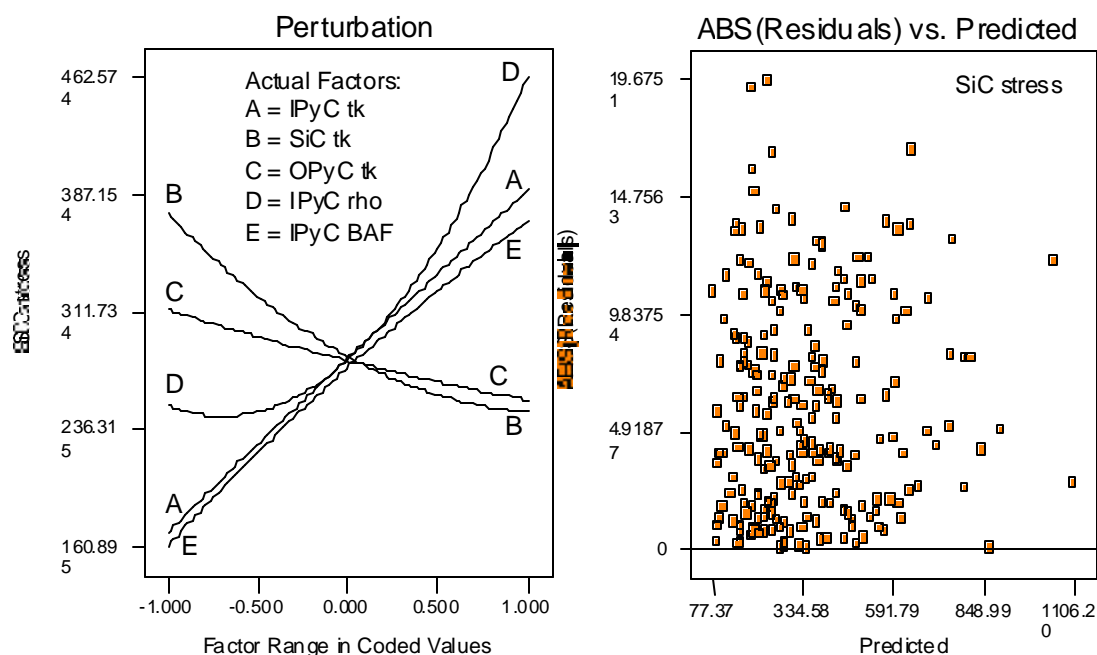


Figure 2-17. Statistical results from 5 parameter, 3 level factorial for the cracked particle.

## 2.4 Mechanical Modeling

The goal of the mechanical modeling effort is to predict the evolution of the mechanical behavior of the fuel particles with burnup as accurately as possible, within the limits of existing data. Additionally, a second goal of the effort is to combine the results of this sub-task with results from fuel/chemistry modeling subtask and to develop a failure model for the fuel. Figure 2-18 schematically illustrates the components of the two models including their interdependencies and interactions.

Historically, stress models calculated the interface stresses between individual layers and failure was assumed to occur due to simple overload of the SiC layer due to internal pressure buildup from fission gas. During operation, the PyC layers undergo shrinkage due to the irradiation exposure. This puts the SiC into compression but puts the PyC layers into tension. As long as the SiC layer remains in compression, failure of the SiC layer is impossible under the old model and assumptions. Failure of the SiC layer, as a pressure vessel, can thus only occur if the internal gas pressure is sufficient to overcome the compressive stress in the SiC induced by the shrinkage of the PyC layers. Since it is assumed that the PyC layers remain in tension, failure by fracture of the SiC layer was not predicted. Yet, failures have been observed in actual fuel with an approximate probability of failure for the NPR fuel of the order of  $10^{-4}$ - $10^{-3}$ . This approach did not accurately predict fuel failure and an alternative approach was sought for this task.

During this reporting period, we have focused on the development of a fracture mechanics based fuel failure model. This model can be used in conjunction with an enhanced Monte Carlo type mechanical model, in an effort to more appropriately represent and predict the failures that occurred in the NPR fuel. The failure model is based on the postulate that SiC failure can occur due to the stress concentration provided by the fracture of the inner PyC layer.

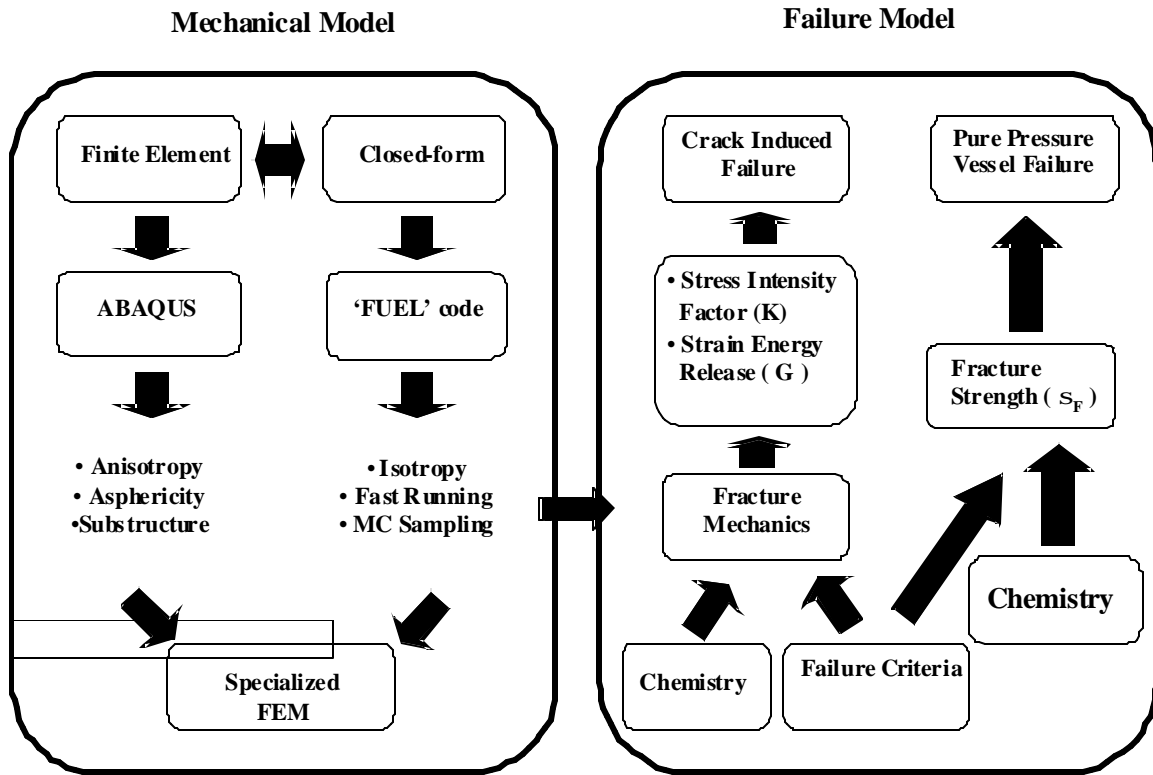


Figure 2-18. Schematic of the mechanical and failure models.

During exposure, the PyC layers will shrink and, at the same time, the kernel internal pressure will increase due to fission gas release. Because of this, there will come a point at which the fracture strength of the inner PyC layer will be exceeded. When this occurs, a radial crack will form in the layer. In our initial formulation of the fracture mechanics based failure model, we treat this crack as being in the composite IPyC/SiC/OPyC layer structure. Further, we assume that the three layers are bound together and act as a monolithic structure. This assumption will be analyzed in detail in the future. Once the IPyC layer cracks it is assumed that a crack of length equal to the IPyC layer thickness exists in the composite. Associated with this crack will be a stress intensity factor,  $K$ . As the internal pressure increases due to fission gas release, the value of  $K$  will also increase. At some point, the value of  $K$  will exceed the fracture toughness of the SiC and fracture will occur. It is also assumed that the OPyC layer fractures when the SiC layer fractures.

Layer thicknesses (kernel, buffer, IPyC, SiC and OPyC) and the densities of the kernel and buffer are all sampled from a common Gaussian distribution with user input mean and variance. The kernel and buffer information are used to calculate moles of fission gas as a function of burnup and thus the internal pressure for the stress analysis. It is assumed that the fracture strength of the PyC can be represented by a Weibull distribution. The cumulative Weibull distribution with mean  $I$  and modulus  $b$  is given by

$$C_{Weibull}(x) = 1 - \exp \left[ - \left( \frac{x}{I} \right)^b \right] \quad (2-1)$$

Equation (2-1) is inverted to give the variate  $x$  as a function of the cumulative distribution:

$$x = \mathbf{I} \exp\{\log[-\log(1 - C_{Weibull})]/\mathbf{b}\} \quad (2-2)$$

The Weibull distribution is generated from Equation (2-2) by sampling a uniform distribution for  $C_{Weibull}$ . The fracture toughness distribution for the SiC is represented by a triangular distribution to reflect the fact that this property can generally be bounded absolutely. A Gaussian distribution would show a tail at either extreme which is unrealistic. The triangular distribution can be represented by:

$$f(x) = \begin{cases} \frac{1}{d^2}(x - m + d) & (m - d \leq x < m) \\ \frac{1}{d^2}(m + d - x) & (m \leq x \leq m + d) \end{cases} \quad (2-3)$$

where  $m$  is the mean value and the standard deviation is given by

$$s = \frac{d}{\sqrt{6}} \quad (2-4)$$

The cumulative distribution is:

$$F(x) = \begin{cases} \frac{1}{2d^2}(x - m + d)^2 & (m - d \leq x < m) \\ 1 - \frac{1}{2d^2}(m + d - x)^2 & (m \leq x \leq m + d) \end{cases} \quad (2-5)$$

The inverse of  $F(x)$  is given as follows:

$$x = \begin{cases} m - d + d\sqrt{2F} & (0 \leq F \leq 0.5) \\ m + d - d\sqrt{2(1 - F)} & (0.5 < F \leq 1) \end{cases} \quad (2-6)$$

In Equation (2-6),  $F$ , which is generated by using a random number generator, is uniformly distributed. Values of  $x$  will fall into a triangular distribution given by Equation (2-3). The complete list of variables used in the Monte Carlo sampling are listed in Table 2-4.

For a sample size of 1,000,000 microspheres and using the parameters in Table 2-4, the model predicts that for the NPR irradiation conditions approximately 595 particles will have cracked IPyC layers. Among this population, 17 particles are predicted to have SiC failure. Based on these numbers the failure probability is estimated to be approximately  $1.7 \times 10^{-5}$ . For reference purposes, the fuel specification required a fuel failure probability lower than  $10^{-4}$ . In 1991, the NPR-1, NPR-2 and NPR-1A capsule irradiation tests<sup>9</sup> yielded particle failure probabilities of approximately  $3.1 \times 10^{-3}$ . The actual failure “probability” is approximately two orders of magnitude higher than the model prediction. However, the trend is in the right direction and future modifications to the model are expected to yield improved performance. It should be remembered that previous models predicted that no failures would occur. These modifications will include improvements to the overall mechanical model to include effects of non-spherical layers and a more accurate model for the evolution of the properties of pyrocarbon during

irradiation including effects of anisotropy in pyrocarbon behavior as a function of burnup. Improvements to the analytical pyrocarbon model have been made to include an irradiation dependence for Poisson's ratio for creep.

Table 2-4. Variables Used in Monte Carlo Sampling Process

Variables	Mean	Standard Deviation	Distribution
Kernel Diameter( $\mu m$ )	195	12	Gaussian
Buffer Thickness( $\mu m$ )	100	10	Gaussian
IPyC Thickness( $\mu m$ )	53	6	Gaussian
SiC Thickness( $\mu m$ )	35	2	Gaussian
OPyC Thickness( $\mu m$ )	43	3	Gaussian
Kernel Density( $g / cm^3$ )	3.43	0.1	Gaussian
Buffer Density( $g / cm^3$ )	0.93	0.05	Gaussian
IPyC Fracture Strength $s_f$ (MPa)	384 (Ref. 10)	8.6 (modulus) (Ref. 11)	Weibull
SiC Critical Stress Intensity Factor $K_{IC} (MPa \cdot \sqrt{\mu m})$	3300 (Ref. 12)	530	Triangular

## 2.5 Fuel Particle Thermal Model

A thermal model has been developed that allows us to evaluate the expected temperature range that the fuel will experience during operation. The model allows the calculation of the fuel temperature distribution for any location within the core. Included are effects of fuel swelling, thermal expansion, fission gas release and buffer densification. Table 2-5 shows the results of these calculations.

The thermal modeling results indicate that there will be a significant variation in fuel temperature as the pebble passes through the core. Because of this temperature variation, there will be large changes in chemical activity as the sphere passes through the core. For example, typical diffusion coefficients will change by 5 to 6 orders of magnitude during the fuel movement from top to bottom. The  $\Delta T$  from the fuel center to the microsphere surface is small, on the order of 20°C at any time or location in the core. The implication of this small change in temperature is that analyses of the chemical behavior of the microsphere can assume average temperatures for each layer at each axial location in the core.

If we compare the expected temperature vs. time history for a nominal microsphere with that of a location in a typical LWR fuel rod we see that there are significant differences. The typical LWR fuel rod will remain at a fixed location for each fuel cycle. Thus, the temperature at a particular position in a LWR fuel rod can be expected to see three (or the number of cycles) periods of approximately constant temperature during its life. However, in the case of the MPBR microsphere, we expect that the fuel's temperature will vary on each pass through the core during its life. The effect of this variation in temperature on the mechanical, time

dependent, behavior of the fuel layers will be complicated and thus, will require accurate modeling if fuel behavior is to be adequately represented.

Table 2-5. Results from Thermal Model Calculations

Pebble Power→ Axial Location→ Loc. In Pebble→ Bulk He Temp.(°C) →	Average Core Inlet Outer Edge 450	Average Core Outlet Center 850	2x Average Core Outlet Center 850
Particle Temperatures (°C)			
Kernel Center	513	968	1074
Kernel Outer Edge	506	961	1067
Buffer Outer Edge	498	952	1056
IPyC Outer Edge	497	951	1056
SiC Outer Edge	497	951	1056
OPyC Outer Edge	497	951	1055
Particle $\Delta T$	16	17	19

## 2.6 Fission Product Behavior Experimental Program

The fission product behavior experimental program is focused on the behavior of silver and palladium. Silver is known to be a fast diffuser in SiC and is released from the coated particle during operation. Palladium is expected to degrade the properties of SiC either by chemical reaction, which thins the SiC layer, or by the production of localized corrosion, which is expected to influence the fracture properties of the layer. Current data for the migration and release of silver from SiC is limited to either high temperature associated with accident conditions or very low temperatures. The database is very limited in the 1000-1600°C. In addition, the diffusion path in SiC will depend on the morphology of the SiC layer. It is expected that a large-grain columnar microstructure will result in enhanced release due to grain boundary diffusion while a fine grain equiaxed microstructure should will slow, but not eliminate, release.

During this reporting period, our effort has been focused on the design and construction of an experiment to study the diffusion of silver in SiC. To this end, two high-temperature furnace systems have been assembled and are in operation. These furnaces will be used to expose silver/SiC diffusion couples for a range of times at temperature in the range 1000-1600°C. A special spherical diffusion couple has been designed and fabricated. This couple, shown in Figure 2-19, consists of a graphite sphere into which silver is deposited. The exterior of the sphere is coated with CVD SiC. A number of diffusion couples have been fabricated and two have already been tested at 1500°C and 1400°C.



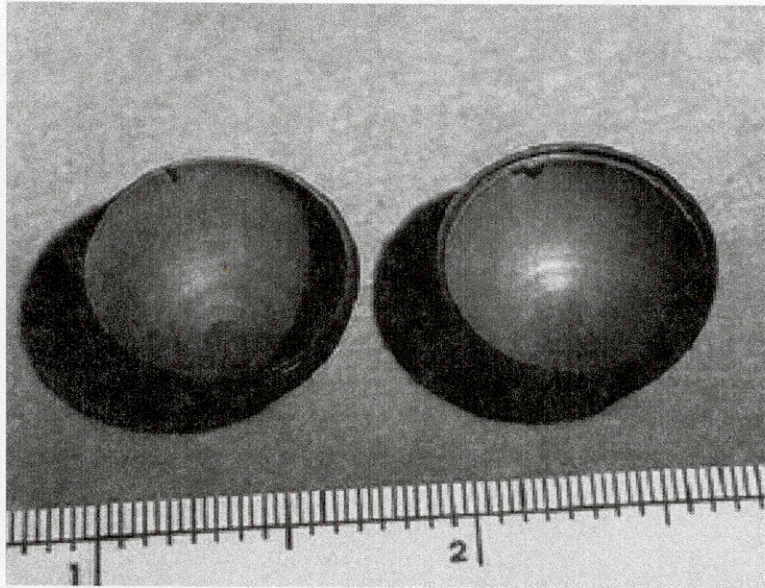


Figure 2-19. Spherical diffusion couple (dimensions are in inches).



### 3. Reactor Physics and Neutronics

The design of a pebble bed reactor (PBR) and the optimization of its in-core fuel cycle require the availability of suitable neutronics methods. Most existing neutronics methods are based on older finite-difference solvers or on statistical methods. Some methods are limited to the “OTTO” (Once Through Then Out) cycle, in which pebbles are not recycled through the core. The OTTO cycle does not fully optimize the use of the pebbles. This is because in the OTTO cycle only the initial composition of the pebbles and their speed within the core are parameters for the optimization process, whereas with recirculation allowed, each subsequent pass through the core offers an opportunity to tailor the pebbles' exposure. A preferable analysis method would perform rapid calculations of steady-state PBR core burnup and flux distributions for scoping studies and for fuel cycle optimization, while allowing the recirculation of pebbles through the core. The method would avoid the shortcomings suffered by existing methods when they are applied to such purposes. For example, existing methods are slow and therefore not suitable for the very large number of repetitive simulations needed for optimization. Furthermore, the statistical methods are even incapable of practically producing useful information for the analysis of non-proliferation characteristics. The new method would incorporate a state-of-the-art nodal neutronics solver and state-of-the-art burnup-corrected nodal depletion with a new algorithm for the recirculation of pebbles. The new method would find the (steady state) asymptotic loading in the reactor directly. The method would also facilitate optimization studies such as searches for optimized fuel utilization and for optimally non-proliferating characteristics of discharged pebbles.

#### 3.1 Neutronics Analysis

The work reported here provides the basis for a comprehensive method to achieve the goals described above. The nodal neutronics solver and depletion modules have not yet been incorporated into the method, but the fundamental approach has been demonstrated.

##### 3.1.1 Core Physics Background

The complete solution of the core physics problem in the pebble bed reactor must simultaneously account for the movement of the fuel, the changing composition of the fuel as it is burned, and the distribution of flux that results from the core geometry and the spatial variation of the composition. This problem has been studied for a long time, and it has been solved in several ways. Massimo<sup>13</sup> gives the basic equation that couples pebble flow to the changing concentration of each nuclide along the flow path. Essentially, this equation is simply the particle balance equation with a convective term added. This equation is written for each nuclide of interest and solved simultaneously with the neutron diffusion or transport equation.

The VSOP code,<sup>14</sup> which is widely accepted as the most appropriate suite of codes for the analysis of PBRs, solves the problem in a time-dependent manner by tracking batches of pebbles which are treated as though they reside for appropriate time periods in successive layers of the core and move discontinuously from each layer to the next. Eventually a steady state may be obtained. The neutronics solver incorporated in VSOP, CITATION, uses the finite-difference method. This solver, though effective for many situations, is two generations of codes and methods older than the state-of-the-art in neutronics solvers. In particular, this method is significantly slower than one based on a nodal solver, and it is thus a less effective tool for frequent repetitive calculations needed for design and optimization. The BURNER/VENTURE codes<sup>15</sup> use a similar approach. Werner<sup>16</sup> very briefly describes a method

that appears similar to VSOP. Jung<sup>17</sup> presents a formal time-dependent solution in one spatial dimension, but he leaves it to the reader to determine the boundary conditions - i.e., the nuclide concentrations at the entry plane. However, some approaches attempt to find a steady-state configuration directly. The KUGEL code<sup>18</sup> treats the distribution of fuel pebbles statistically, characterizing them by burnup as correlated with exposure. A complicated logic summarized by Massimo<sup>13</sup> leads to the determination of a steady state. Izenson<sup>19</sup> also uses a statistical approach, coupled with VSOP for the flux calculations, to find a steady state and evaluate the probability of finding "hot spots" in which groups of pebbles of higher-than-average power are clumped together. The PREC<sup>20</sup> and PREC2<sup>21</sup> codes obtain a steady state directly for the OTTO cycle, in which pebbles are not recycled. These codes allow tracking of pebbles along curved streamlines. However, the time-dependent codes and the statistical methods require extensive calculations, and the OTTO cycle is not general enough for design optimization of the PBR. An efficient computational method is needed for a PBR with recirculating fuel.

Another reason for the adoption of a deterministic approach is the elimination of the additional uncertainty inherent in statistical methods. Whereas no method can be immune from the uncertainty that arises from the random aspects of the loading pattern, the use of statistical methods adds uncertainties that stem from the solution method. The elimination of these additional uncertainties is ensured by the use of deterministic methods. Therefore, the benefits of using deterministic methods include a better estimation of the safety margin parameters for the reactor. They also include a significant reduction of the computational effort for comparable results.

The assumption of the steady state requires that the burnup be time-invariant at each point. Thus, the burnup distributions on the entry and exit planes must be time-invariant, and the difference between the burnup values at the entry and exit points on a pebble flow streamline is equal to the additional burnup increment the pebbles accumulate along the streamline. For any specific rule governing the removal and recycling of pebbles (e.g., all pebbles exceeding a cutoff burnup are removed, and those not removed are reintroduced randomly), and for given reactor power, reactor geometry, new pebble composition, and pebble flow speed distribution, we anticipate that the burnup distribution at the entry plane is unique. We have found a method of finding this burnup distribution at the entry plane and, along with it, the self-consistent solution for the neutron flux, the burnup distribution, and the fissile nuclide concentrations throughout the core. A method that fulfills these requirements and generates the desired self-consistent solution is discussed in the next section. In future work, this method will be extended to more realistic reactor configurations and will be adapted to incorporate a state-of-the-art nodal diffusion solver. This self-consistent solution can then be exploited to evaluate the various parameters that define the reactor performance, including neutron and fuel economy, safety and shutdown margins, and optimal non-proliferation characteristics of the discharged pebbles.

### 3.1.2 Description of the Model

We let  $B(\vec{r}, t)$  be a variable that characterizes the average burnup of the mixture of pebbles located at position  $\vec{r}$  at time  $t$ . This variable may or may not have the conventional units of energy per unit mass (e.g., MWd/MTHM). We can write a conservation equation for  $B$ :

$$\frac{\partial B(\vec{r}, t)}{\partial t} = F(\vec{r}, t) - \nabla \bullet (B(\vec{r}, t) \cdot \vec{u}(\vec{r}, t)) \quad , \quad (3-1)$$



where  $F(\vec{r}, t)$  is an appropriately normalized fission rate. This equation is similar to the equation given by Massimo<sup>13</sup> for nuclide concentrations, but it is written for the burnup variable, to which the nuclide concentrations are related.

Assuming a steady state with purely axial flow, introducing a normalization constant  $A$ , and integrating from the entry plane ( $z=0$ ), we obtain

$$B(x, y, z) = B_0(x, y) + \frac{A}{w(x, y)} \int_{z=0}^z \Sigma_f(x, y, z') f(x, y, z') dz' \quad (3-2)$$

where  $B_0(x, y)$  is the burnup distribution at the entry plane.

In Equation (3-2), the flow speed  $w(x, y)$  is assumed to be known from a separate calculation or measurement. To first order, the fission cross section is a function of burnup. The neutron flux is obtained from the neutron diffusion or transport equation, in which burnup-dependent composition data appear in the coefficients. So if the entry-plane burnup is known, the burnup distribution, the related quantities, and the neutron flux can be found directly by an iterative numerical scheme.

In the OTTO cycle, the entry-plane burnup is identically zero. However, when pebbles are recirculated, the entry-plane burnup depends on the procedure governing the recirculation process, and on the burnup increments accrued by pebbles on successive passes through the core. So the entry-plane burnup becomes another unknown quantity to be determined in the iteration scheme; the rule for the recirculation procedure provides the extra information needed for finding the additional unknown quantity.

The solution starts by assuming that the burnup is zero throughout the core and calculating the neutron flux distribution with the diffusion or transport solver. Then the burnup and associated composition are found from Eq. (3-2) under the assumption that the entry plane burnup is still zero. The solution is still not self-consistent, because the neutron flux was not obtained from the compositions calculated in the last step. Furthermore, except in the OTTO cycle, the entry-plane burnup has not yet been found.

Next, a double iteration loop is begun in which the inner iteration converges on the neutron flux and the burnup below the entry plane, and the outer iteration converges on the entry-plane burnup. The algorithm for the outer iteration depends on the rule governing pebble recycling.

The method does not require the solution variables to follow a physically meaningful sequence of states, but only to converge to a physically meaningful configuration. Thus, for well-chosen initial guesses, convergence has been obtained in a few iterations in one-dimensional problems. This behavior permits the new method to calculate steady states much more rapidly than methods, which follow actual sequences of transient states to asymptotic steady states.

### *One-Dimensional Models*

This approach has been applied successfully to a one-dimensional model of the OTTO cycle and to a one-dimensional model in which each pebble is examined when it exits the core after each pass; pebbles with burnup in excess of a cutoff value are discarded and replaced by fresh pebbles. This case with recycling is described below.

The equation for the entry-plane burnup is found by following the accumulation of burnup in a

single pebble as it makes repeated trips through the core. If a pebble is removed when its burnup exceeds the cutoff value  $B_{\max}$ , and  $m_{\max}$  trips through the core are required for this, then it is found that the average burnup of the mixture of recycled and new pebbles at the entry plane is

$$\bar{B}_o = \frac{1}{m_{\max}} \sum_{m=1}^{m_{\max}-1} B^{(m)}(H) \quad (3-3)$$

where  $z=H$  is at the bottom of the core, and where  $B^{(m)}(H)$  is the burnup of an individual pebble at the end of its  $m^{th}$  pass. This equation relies on the assumption that the number of pebbles in any core layer which are making their  $m^{th}$  pass is the same for all  $m$  less than or equal to  $m_{\max}$ . The value of  $m_{\max}$  can be found from the core thermal power  $P$  and the number of pebbles  $n_p$  in the core as

$$m_{\max} \geq \frac{c B_{\max} w n_p}{P H} \quad (3-4)$$

where  $c$  is a units conversion factor, and where the value computed by Eq. (3-4) is rounded up to the next integer.

The values of  $B^{(m)}$  are found in terms of the number density  $N$  of fuel nuclei:

$$B = (N_o - N)A \quad (3-5)$$

By following the consumption of fuel nuclei in a pebble during successive passes through the core, and applying Eq. (3-5), we find that

$$B^m(H) = N_o A \left\{ 1 - \exp \left[ \frac{-m S_f}{w} \int_{z=0}^H f(z) dz \right] \right\} \quad (3-6)$$

and

$$\bar{B}_o = \frac{N_o A}{m_{\max}} \sum_{m=1}^{m_{\max}-1} \left\{ 1 - \exp \left[ \frac{-m S_f}{w} \int_{z=0}^H f(z) dz \right] \right\} \quad (3-7)$$

### *Two-dimensional Model*

The approach described above is extended to cylindrical coordinates by writing the neutron flux, the burnup function, and the compositions as functions of  $r$  and  $z$  and allowing the pebble flow speed to vary with  $r$ . It is assumed that the pebble flow is axial and laminar. The neutron flux solution is obtained as a function of  $r$  and  $z$ .

Before an equation for the entry-plane burnup can be obtained, a rule must be selected to govern the recycling of pebbles. We have obtained solutions for two different recycling rules. In both cases, a maximum value of burnup  $B_{\max}$  is imposed, and pebbles emerging from the exit plane with burnup values exceeding this cutoff are discarded and replaced with fresh pebbles. First, we solved for the case in which a given pebble makes every pass through the core in the same radial zone, which is narrow enough that all properties in the zone are radially uniform. Then we solved for the case in which the recycled pebbles are thoroughly mixed, both with each other and with fresh pebbles, before being introduced again at the entry plane.

For the first case, there is a different maximum number of passes in each radial zone; for radial zone  $j$ ,

$$m_{\max j} \geq \frac{cB_{\max} w_j n_{pj}}{P_j H} \quad (3-8)$$

where  $m_{\max j}$ ,  $w_j$ ,  $n_{pj}$ , and  $P_j$  are, respectively, the maximum number of passes, the axial flow speed, the number of pebbles, and the power in the  $j^{\text{th}}$  radial zone. Then the solution in each radial zone follows the one-dimensional solution, becoming

$$\bar{B}_{o,j} = \frac{N_o A}{m_{\max j}} \sum_{m=1}^{m_{\max j}-1} \left\{ 1 - \exp \left[ \frac{-m S_f}{w_j} \int_{z=0}^H f_j(z) dz \right] \right\} \quad (3-9)$$

For the second case, it is not possible to follow individual pebbles on repeated trips through the core, because they are distributed probabilistically over the entry plane on successive trips. Izenzon<sup>7</sup> addressed this problem with an elegant and sophisticated probabilistic treatment. We treat the problem by averaging over the flow distribution.

The average number of passes a pebble makes through the core before reaching the burnup limit is

$$\bar{m}_{\max} \geq \frac{cB_{\max} \bar{w} n_p}{P H} \quad (3-10)$$

The flow-averaged number density of fuel nuclei in pebbles completing their  $m^{\text{th}}$  pass is:

$$\bar{N}^{(m)}(H) = \frac{\int_{r=0}^R r w(r) \bar{N}^{(m-1)}(H) \exp \left[ \frac{-S_f}{w(r)} \int_{z=0}^H f(r,z) dz \right] dr}{\int_{r=0}^R r w(r) dr} \quad (3-11)$$

where  $R$  is the core radius. For  $m=1$ ,  $\bar{N}^{(m-1)}(H) = N_o$ , the number density of fuel nuclei in fresh pebbles. Then the average entry-plane burnup is

$$\bar{B}_o = \frac{A}{\bar{m}_{\max}} \sum_{m=1}^{\bar{m}_{\max}-1} \left\{ N_o - \frac{\int_{r=0}^R r w(r) \bar{N}^{(m-1)}(H) \exp \left[ \frac{-S_f}{w(r)} \int_{z=0}^H f(r,z) dz \right] dr}{\int_{r=0}^R r w(r) dr} \right\} \quad (3-12)$$

Equation (3-12) is evaluated by first using Eq. (3-11) successively for all values of  $m$  from 1 to  $m_{\max}$  to calculate all the values of  $\bar{N}^{(m-1)}(H)$  that contribute to the sum.

### Convergence

When Eq. (3-2) is solved iteratively for  $B(x,y,z)$ , the flux  $f(x,y,z')$  has already been found for the cross-section distribution  $\Sigma_f(x,y,z')$  determined in the previous iteration cycle for  $B$ . The cross-

section function is dependent on burnup, and it can be written

$$\Sigma_f = \mathbf{a} + \mathbf{b} B(x, y, z') \quad (3-13)$$

So Eq. (3-2) can be rewritten

$$B(x, y, z) = B_o(x, y) + \mathbf{a} \int_{z'=0}^z \mathbf{f}(x, y, z') dz' + \mathbf{b} \int_{z'=0}^z B(x, y, z') \mathbf{f}(x, y, z') dz' \quad (3-14)$$

or

$$B(x, y, z) = \mathbf{y}(x, y, z) + C \int_{z'=0}^z B(x, y, z') \mathbf{f}(x, y, z') dz' \quad (3-15)$$

where C is a constant and  $\mathbf{y}$  is a known function of  $(x, y, z)$ . The integration in Eq. (3-15) is performed while  $x$  and  $y$  are held fixed, so  $x$  and  $y$  may be regarded as constant. Since the iterations for  $B$  do not alter the flux,  $\mathbf{f}(x, y, z')$  may also be treated as a constant, and furthermore since  $\mathbf{f}(x, y, z')$  is continuous in  $0 \leq z \leq H$ , the flux is bounded:

$$|\mathbf{f}(x, y, z)| \leq \Phi_m(x, y) \quad (3-16)$$

where  $\Phi_m$  is the maximum value of  $\mathbf{f}(x, y, z)$  in  $[0, H]$ .

It follows that the kernel  $K = B\mathbf{f}$  in the integral in Eq. (3-15) satisfies the Lipschitz condition:

$$|K(x, y, z; B_2(x, y)) - K(x, y, z; B_1(x, y))| \leq \Phi_m(x, y) |B_2(x, y) - B_1(x, y)| \quad (3-17)$$

### 3.1.3 Results

The PEBBED code was written to solve for the coupled neutron flux and burnup in accordance with the method described above. In the one-dimensional option, the flux is found by a direct matrix inversion solution of the one-group diffusion equation. A sample problem was selected from Reference 7; the problem parameters are:

**MPBR Base Case**  
(Izenson (Reference 19 p.283))

Power (MWt)	200
Core Height (m)	9.43
Core Radius (m)	1.50
Enrichment	7.3%
Heavy Metal Loading (g/pebble)	7.0
No. of Pebbles	360,000
Burnable Poison	None
Discharge Burnup (MWD/MTU)	82000
Average Pebble Velocity (m/day)	0.13824
Average No. of Passes before discharge	15 (15.1)

#### 1-D Results

$m_{max}$

16

Entry Plane Burnup (GWD/MTU)	46.2
Exit Plane Burnup (GWD/MTU)	50.5
Peak/Average Axial Power Density Ratio	1.58

The ratio of peak and average axial power density and the ratio of peak and mean neutron flux are shown in Figure 3-1. The peaks are slightly shifted towards the top because the fuel burnup is slightly lower at the top, so that there are more fuel nuclei near the top. The average burnup distribution is shown in Figure 3-2.

Figure 3-3 shows the way that the burnup of a single pebble increases on successive passes through the entry plane. In the one-dimensional model, all pebbles experience identical histories, so this burnup history is the same for all pebbles. In contrast, the burnup distribution in Figure 3-2 is the average, at each point, of the burnup values of all the pebbles at that point; at each point there are equally many pebbles with all possible numbers of prior passes from 0 (pebbles on their first pass) to  $m_{max}-1$  (pebbles on their last pass).

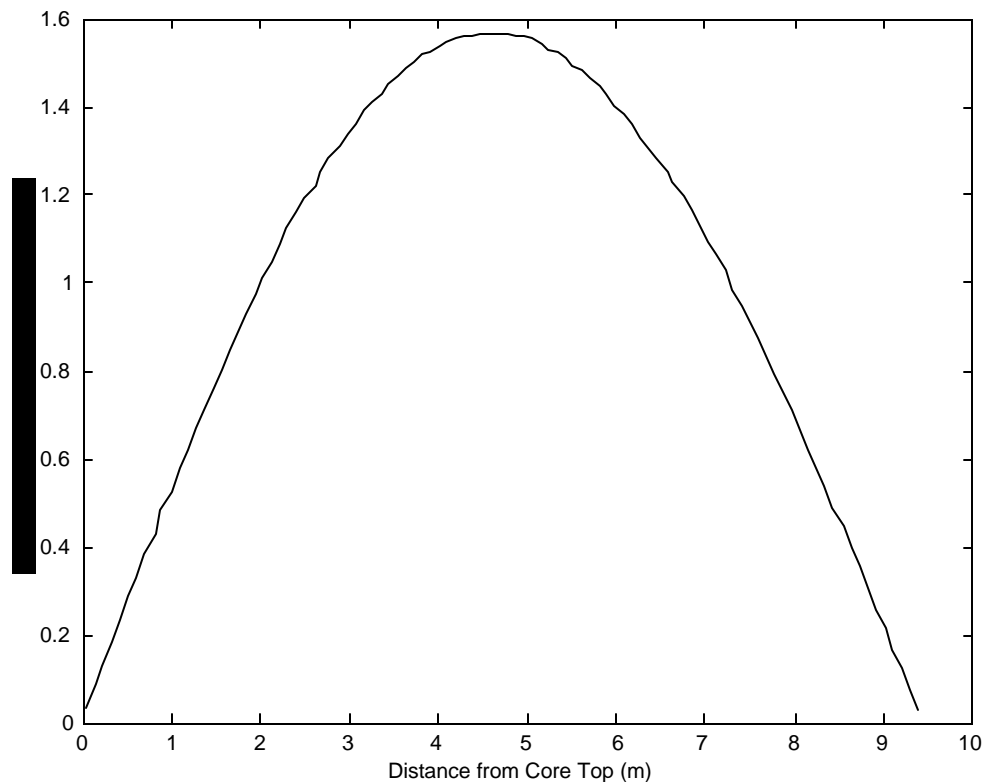


Figure 3-1. Ratios of peak and average axial power density and peak and average neutron flux.

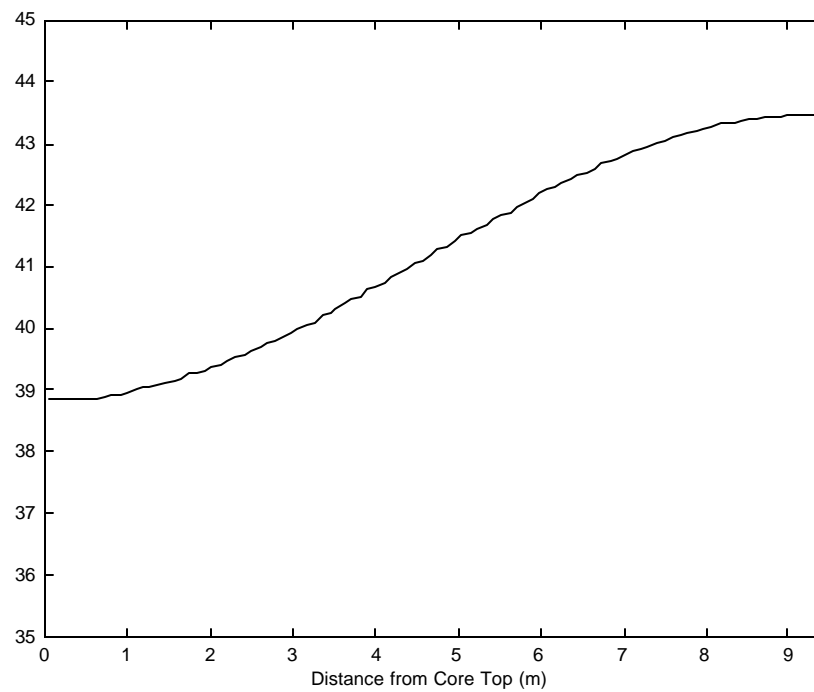


Figure 3-2. Axial distribution of average burnup.

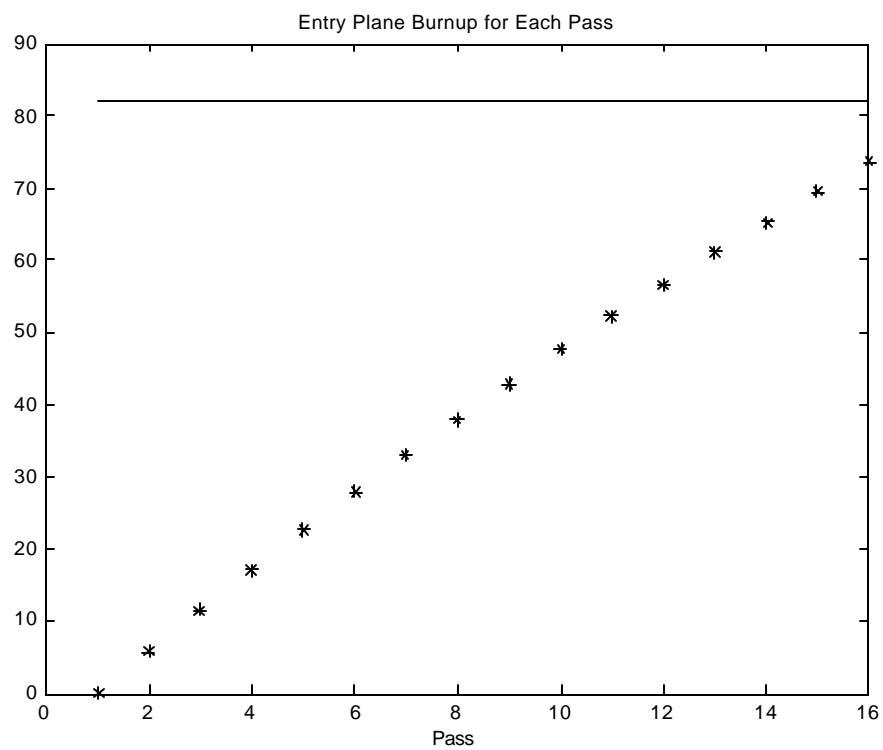


Figure 3-3. The entry-plane burnup of a pebble on successive passes.

## 2-D Results

Two procedures for recycling pebbles were considered. In the first, the cylindrical core region was divided into fifteen equally wide annular regions, and it was stipulated that any particular pebble would be reintroduced repeatedly into the same annular region. The composition and burnup in a given annular region were assumed to be uniform across the width of the region but to vary with axial position. If the regions are sufficiently narrow, this assumption is reasonably accurate, and the solution is otherwise exact. This procedure is identified as "channeling" in the discussions below.

In the second procedure, all the pebbles passing through the exit plane with burnup values less than  $B_{max}$  are mixed thoroughly, together with fresh pebbles replacing those that were removed for having burnup values greater than  $B_{max}$ . This mixture of pebbles is then distributed over the entry plane so that the volumetric flow rate at each point in the cross section remains time-invariant. Because the succession of radial zones a particular pebbles occupies can only be handled statistically (as in Izenson's analysis<sup>7</sup>), the number of passes a pebble makes before reaching  $B_{max}$  is not the same for all pebbles, and  $m_{max}$  is computed for the average pebble. This procedure is identified as "random" in the discussions below.

For each of the two recycling procedures, analyses were performed for uniform and parabolic velocity profiles. The data characterizing the four cases are given in Table 3-1 below.

In accordance with the definition of the burnup variable, the label "maximum exit plane" burnup in Table 3-1 means the maximum value of the burnup of the mixture of pebbles emerging from any point in the exit plane. The burnup value associated with any point in the reactor is always the average value of the burnup in the mixture of pebbles there, in which pebbles are present that have made various numbers of previous trips through the core.

Table 3-1. Parameters for 2-D Calculations

	Case 1	Case 2	Case 3	Case 4
Velocity Profile	uniform	parabolic	uniform	parabolic
Reload Scheme	channeling	channeling	random	random
Burnup (GWD/MTU)				
mean at entry plane	45.1	45.0	45.2	51.9
mean at exit plane	49.6	50.0	49.6	56.5
maximum at exit plane	52.6	51.8	52.4	58.9
discharge limit	82.0	82.0	82.0	82.0
Peak/Average Power	2.62	2.63	2.59	2.67
Average No. of Passes before Discharge	18	15	16	16

*Cases 1 and 2: A pebble is always recycled through the same radial zone*

Figures 3-4 and 3-5 display the calculated power and burnup distributions for Case 1. In these plots, only the ridges and valleys are meaningful, since the compositions and burnup values are assumed uniform across each radial zone. The ridges and valleys represent the average values in the radial zones, and the surfaces connecting ridges and valleys are just artifacts of the plotting software. Figures 3-6 and 3-7 show the same quantities for Case 2.

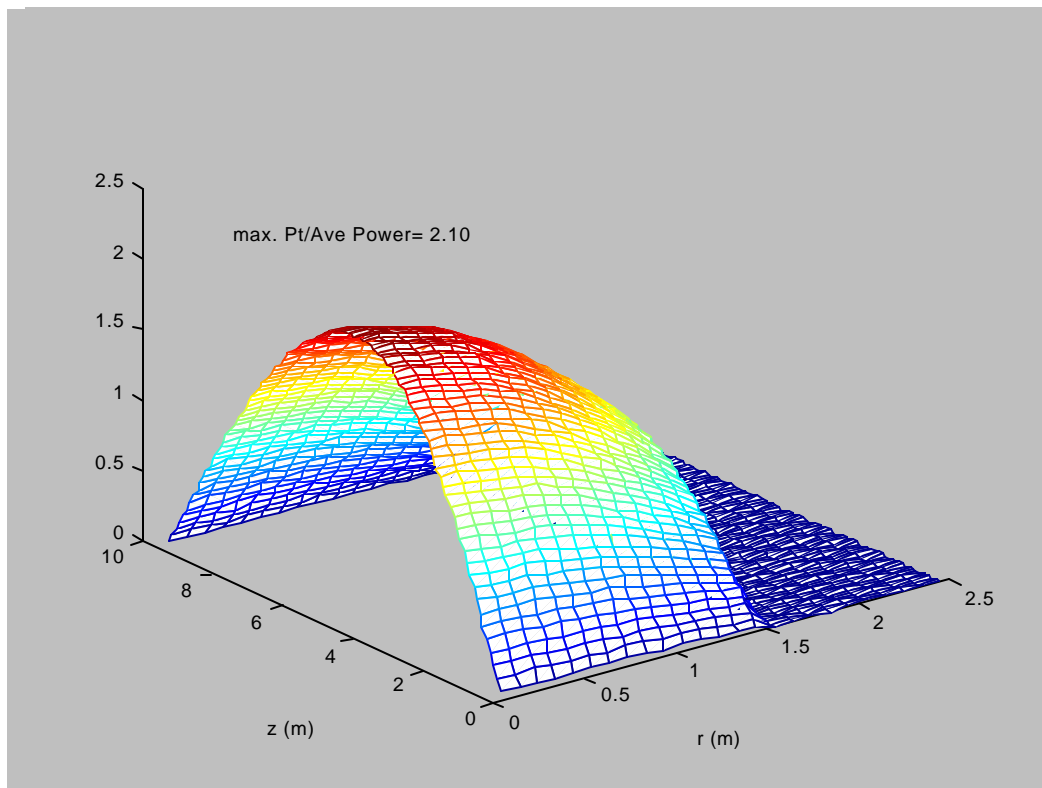


Figure 3-4. Power distribution for Case 1.

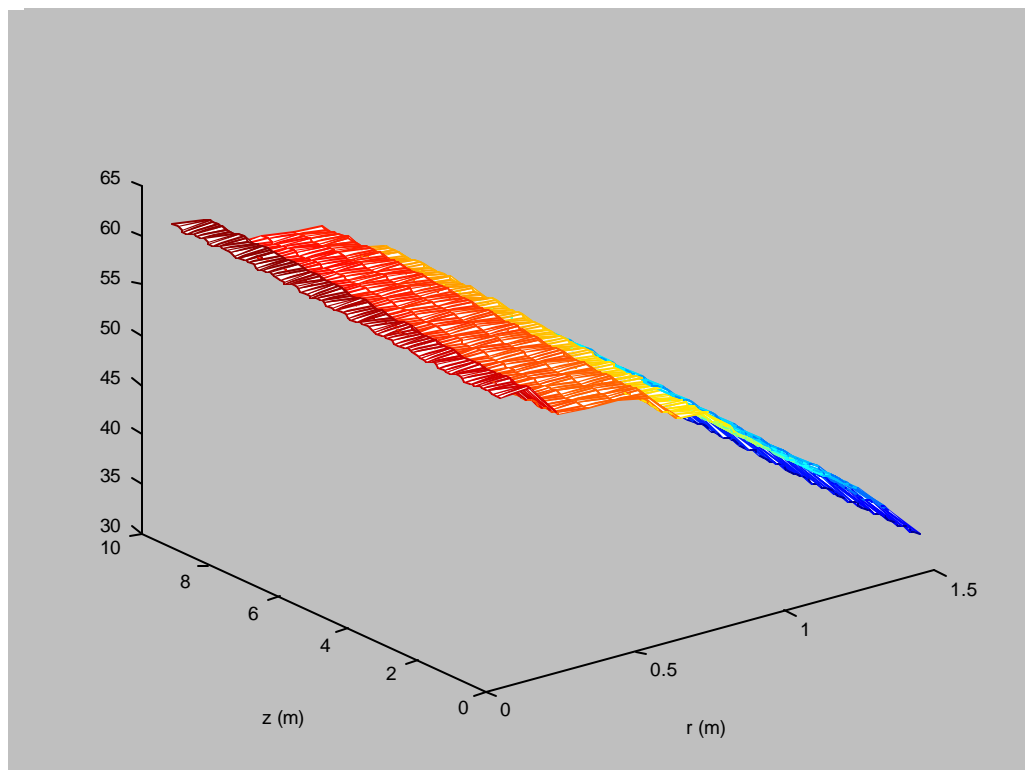


Figure 3-5. Burnup distribution for Case 1.



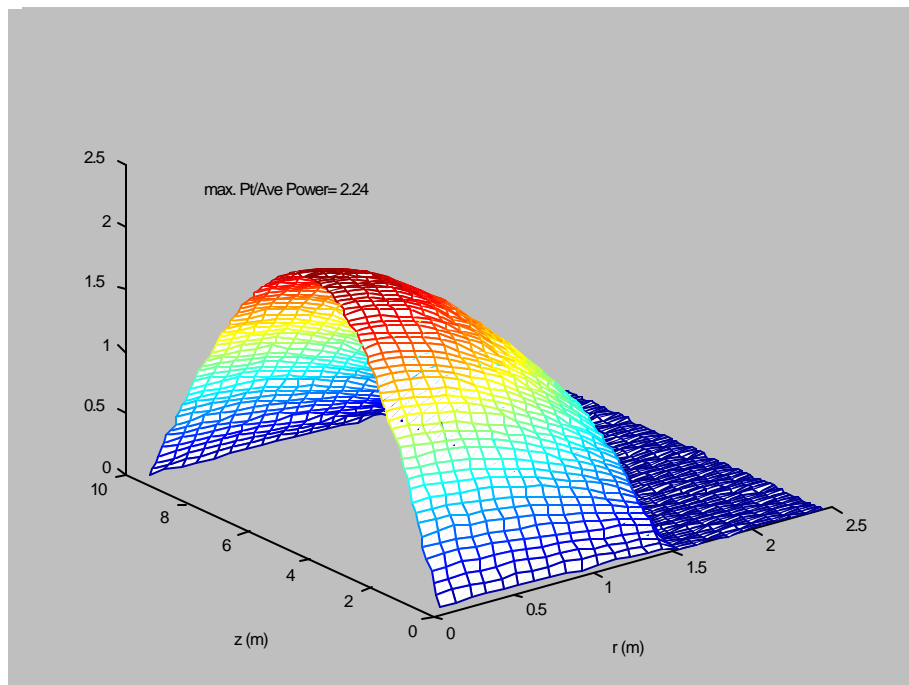


Figure 3-6. Power distribution for Case 2.

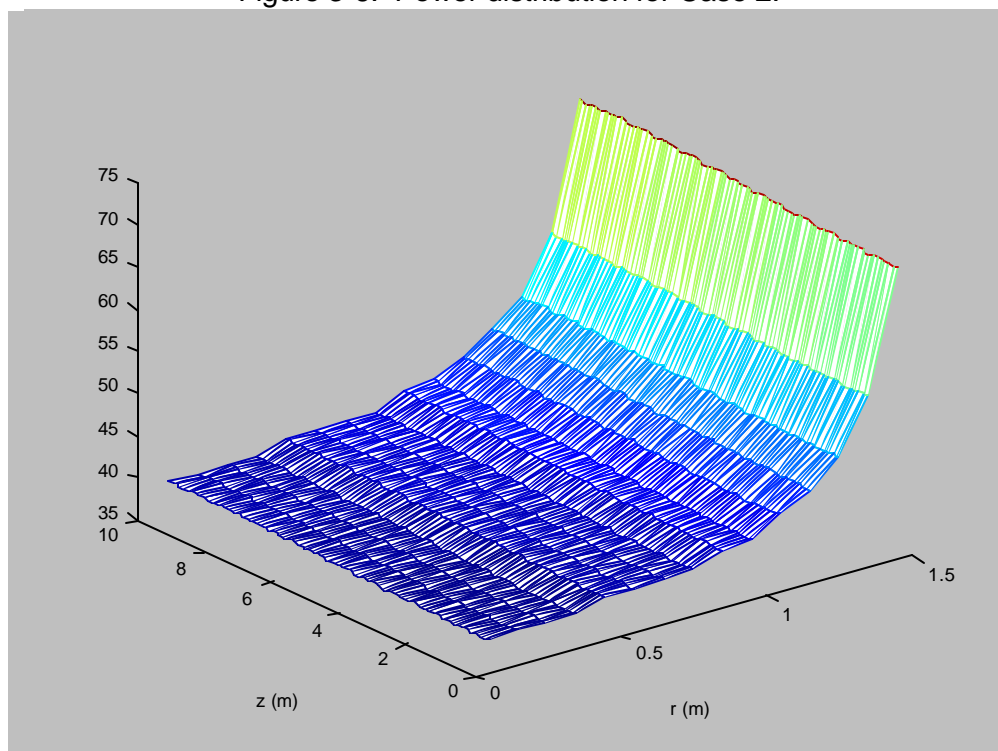


Figure 3-7. Burnup distribution for Case 2.

Figure 3-8 shows the radial burnup profiles in the axial midplane for Cases 1 and 2. In Case 1, where the velocity is uniform, pebbles all spend equal times in transit, so the pebbles closer to the cylindrical axis, where the power is higher, are burned up faster. Since these pebbles remain in the same channels in each trip through the core, the average burnup is higher in the central channels.

In Case 2, where the velocity is higher near the axis, even though the pebbles near the axis are exposed to a higher power level than pebbles near the periphery, they spend less time in a single pass through the core. These effects are roughly in balance across the core, producing a uniform burnup profile. Although at the outer boundary where pebbles are moving most slowly, the burnup is slightly higher. At the bottom of the core, the effect of the low speed near the radial boundary is more pronounced, as seen by comparing Figures 3-5 and 3-7. The burnup is substantially greater near the radial boundary at the exit plane in this case.

#### *Cases 3 and 4: Random Recycle*

In Cases 3 and 4, all the pebbles emerging from the exit plane at less than the burnup limit are mixed together with each other and with new pebbles that replace those removed for having burnup values above the burnup limit. Figures 3-9 and 3-10 show the power and burnup distributions for Case 3, and Figures 3-11 and 3-12 show the same quantities for Case 4. The most dramatic difference is seen between Figure 3-10 and Figure 3-12. As for pebble channeling, when the velocity profile is uniform, the burnup is greater near the cylindrical axis, because the neutron flux is higher there. But when the velocity profile is parabolic, the longer transit time near the radial boundary causes the burnup to increase more along the flow path there than near the axis, even though the neutron flux is higher near the axis. Figure 3-13 shows this difference at the axial midplane, but the effect is considerably greater near the exit plane, as it was for the case of pebble channeling.

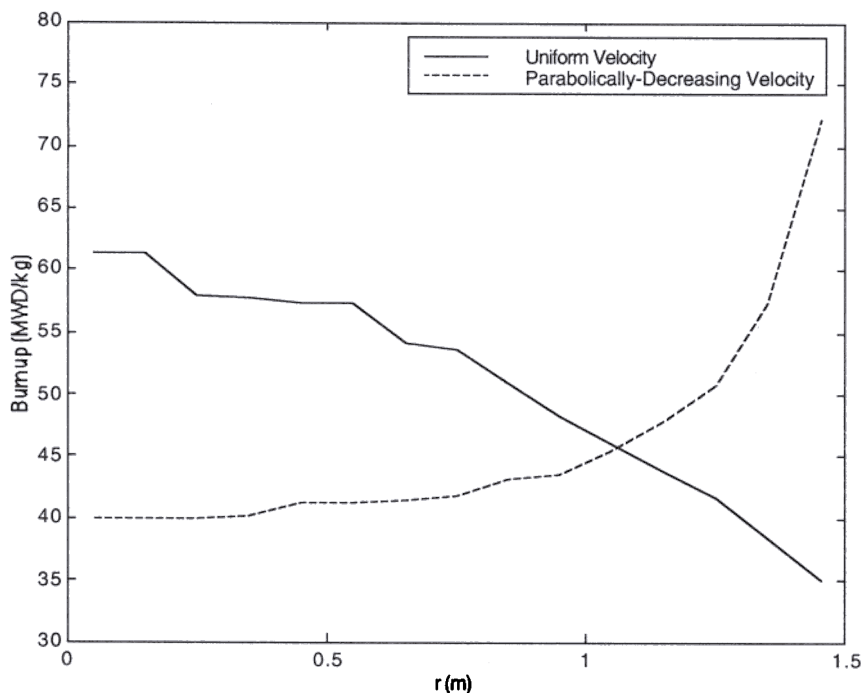


Figure 3-8. Burnup across axial midplane for Cases 1 and 2.

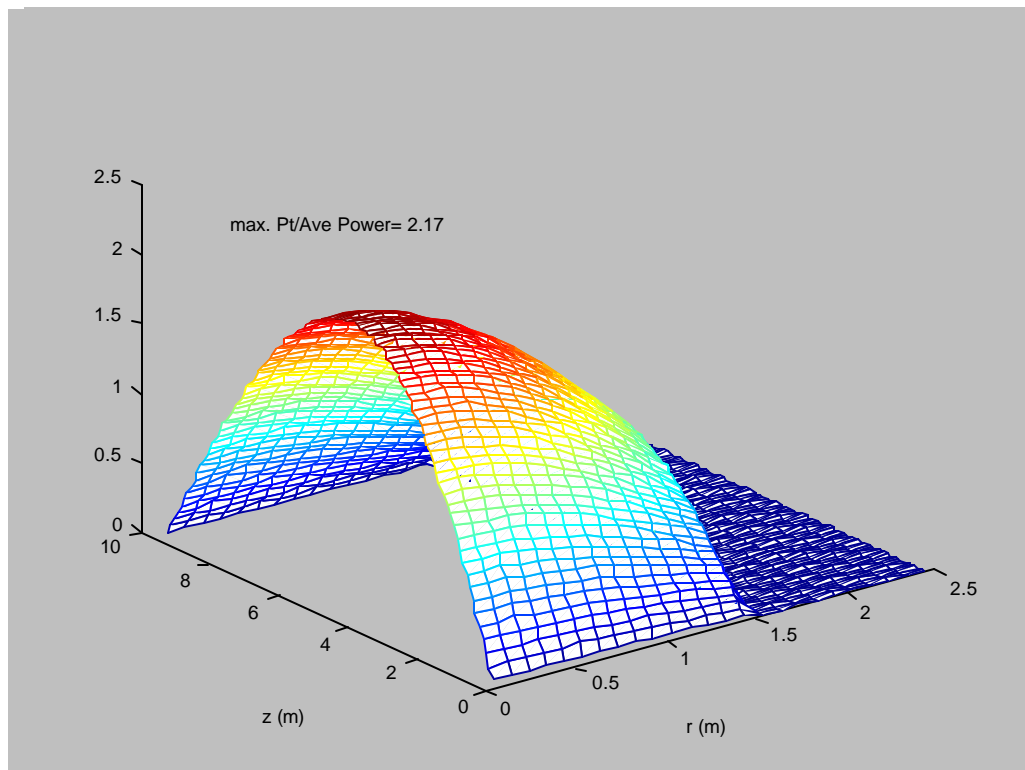


Figure 3-9. Power distribution for Case 3.

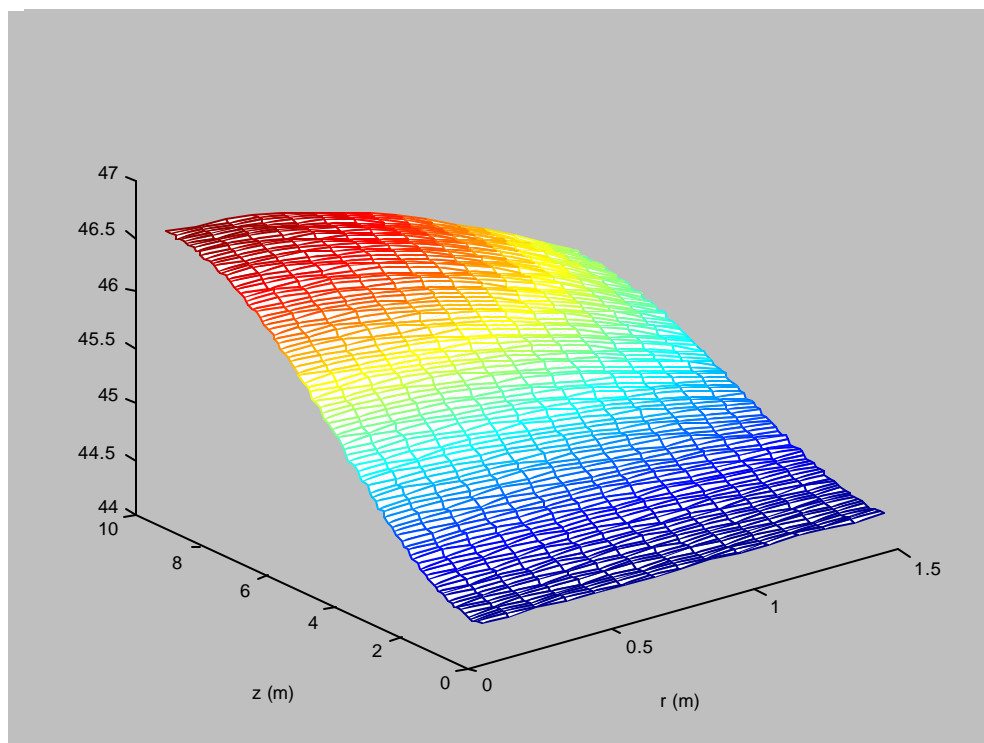


Figure 3-10. Burnup distribution for Case 3.



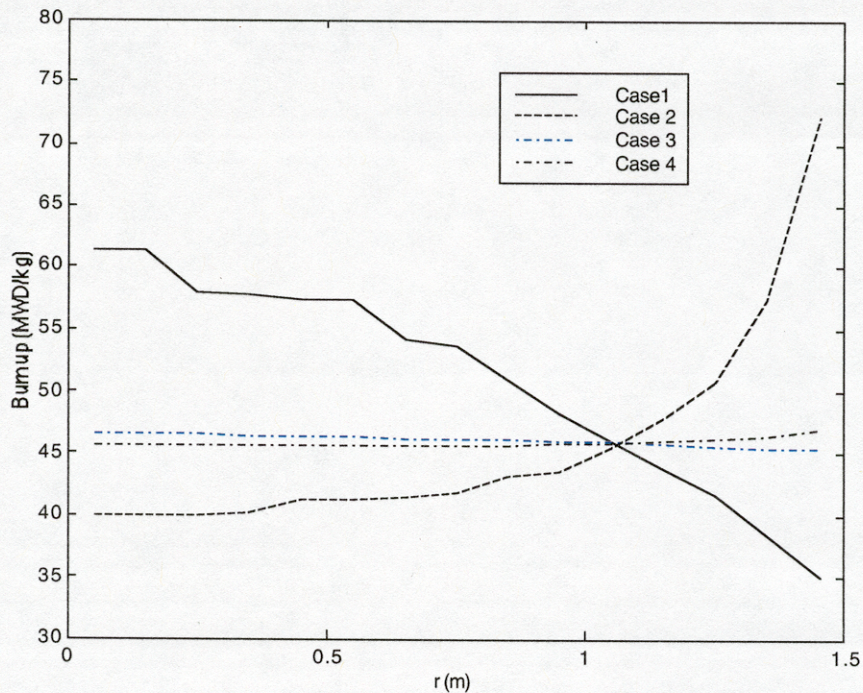


Figure 3-13. Burnup across axial midplane for Cases 1 through 4.

#### *Comparison With Statistical Solution*

The results of Case 3 are compared in Figures 3-14 and 3-15 with Izenson's<sup>7</sup> results for a similar problem. The figures show the two solutions for the power density on the axis of the core. Izenson assumed a reflector at the bottom of the core, but both solutions show similar shifts of the power towards the top of the core where the fuel is fresher. Given that the boundary conditions are different, the two solutions are similar. In particular, the two solutions have their peak values at nearly the same position.

We have demonstrated a powerful method that can be used to find self-consistent solutions for the neutron flux and the burnup in a pebble-bed reactor with arbitrary velocity profile. It can be used for any recycling procedure that can be characterized quantitatively, although in many cases this procedure must be modeled in terms of average quantities. In such cases, the results still compare well with solutions obtained from more rigorous statistical methods. It remains to implement the method with accurate multigroup neutronics tools. The work to date has shown that the method converges to physically realistic solutions.



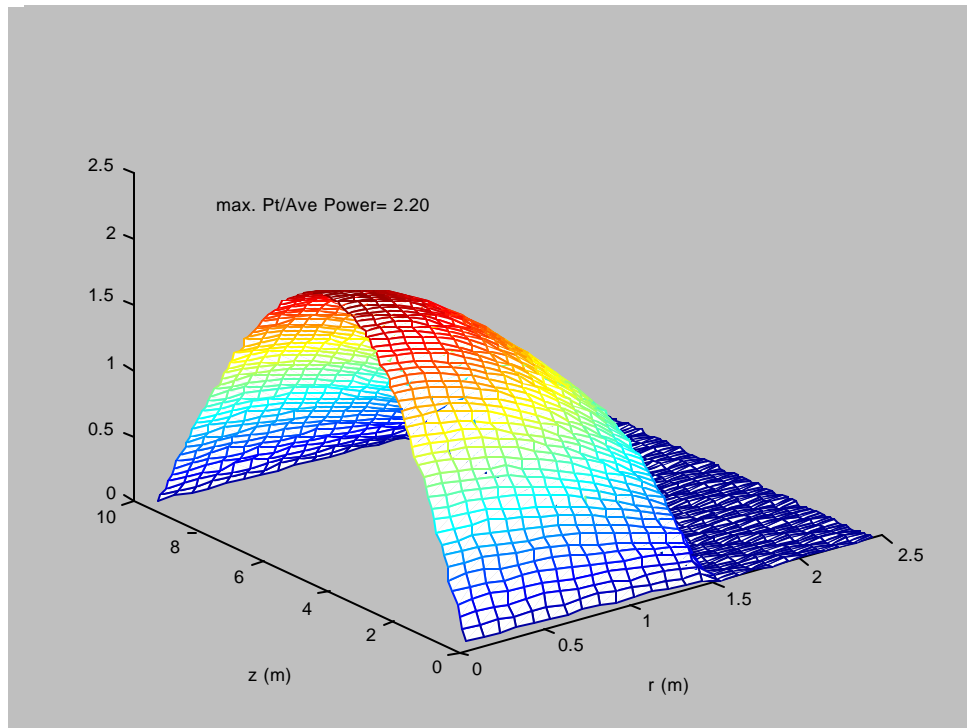


Figure 3-11. Power distribution for Case 4.

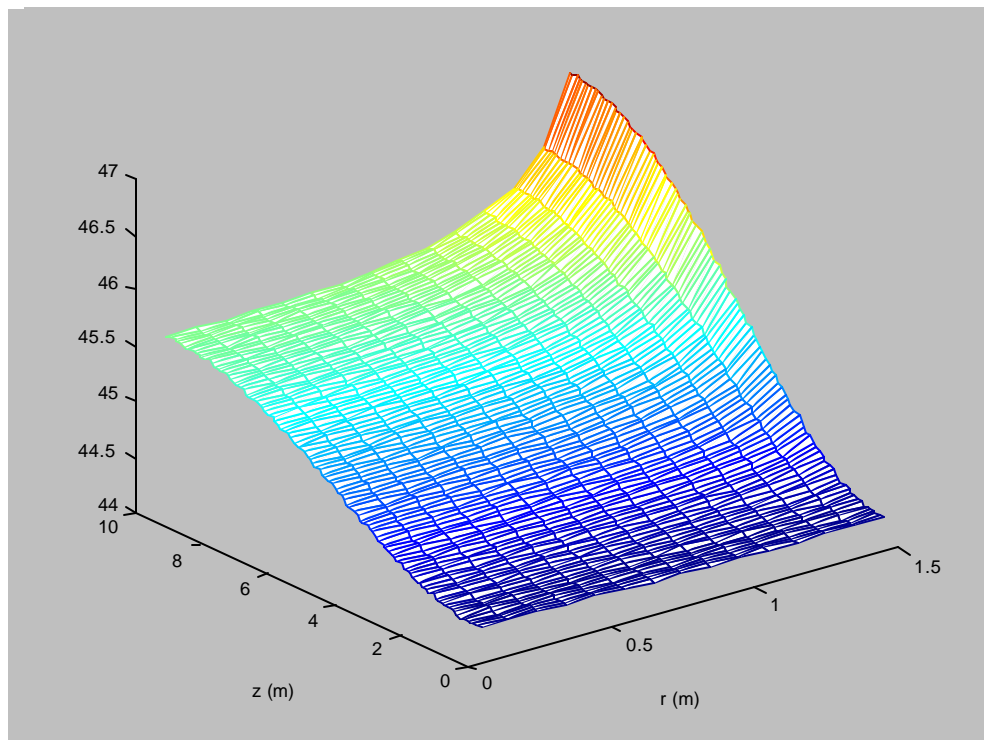


Figure 3-12. Burnup distribution for Case 4.

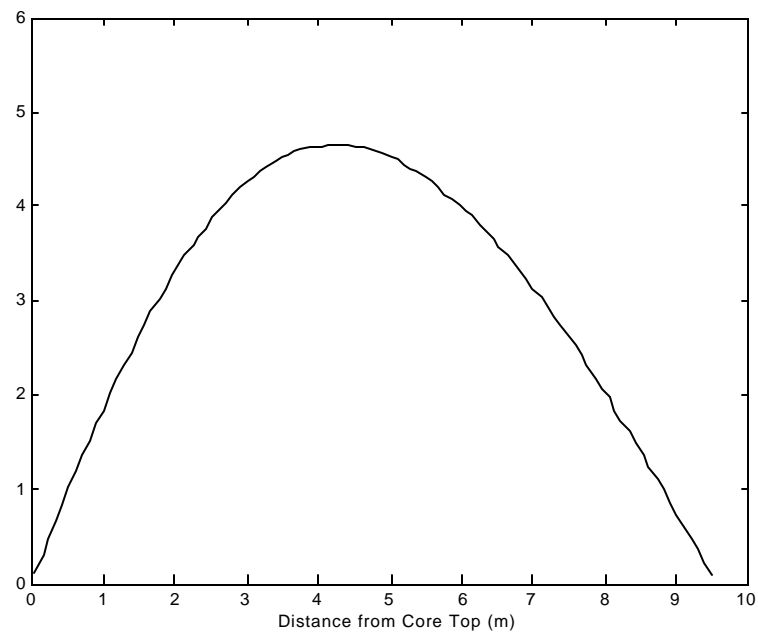


Figure 3-14. Power density on the core axis in Case 3.

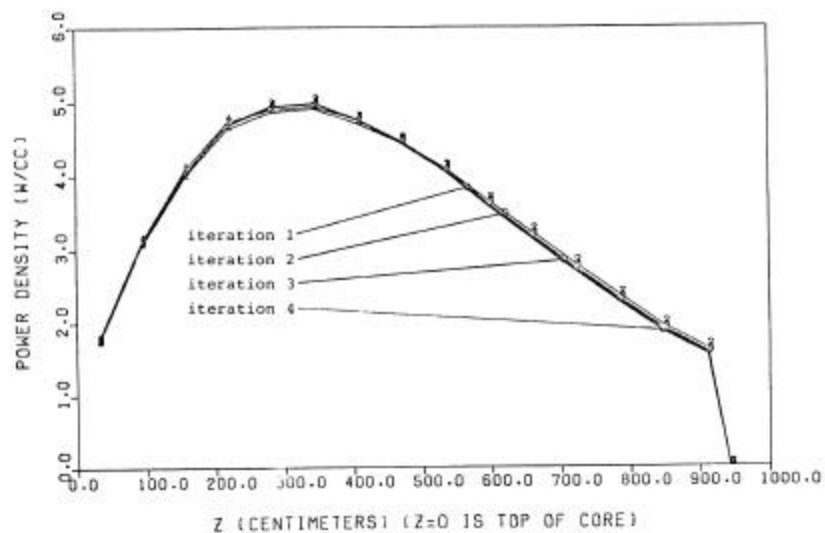


Figure 3-15. Power density on the core axis from Izenson's solution.

## 3.2 Reactor Physics

The initial goal of the reactor physics task is the development of modern software tools for the neutronic design and analysis of pebble bed reactors (PBRs). A validated set of such tools is needed for the design, construction and licensing of a modular PBR in the US. In this project, we use both conventional diffusion-theory methods (as discussed in the previous section) and advanced Monte Carlo techniques.



Previous physics codes have relied on diffusion theory, with provisions for the special nature of pebble-bed cores. Several such codes are available, the best known being VSOP. The VSOP code was developed for the German AVR program, and was subsequently adopted for use in both the South African PBMR and the Chinese HTR-10 reactor projects. VSOP consists of a comprehensive suite of modules for modeling neutronics, fuel management, thermal hydraulics and fuel cycle economics. VSOP (version '94) has been implemented at MIT and is being used to evaluate the proliferation resistance of various fuel cycles. However, the code is old fashioned, poorly documented and not very "user friendly."

Advances in computer hardware are now making it possible to apply Monte Carlo codes to the modeling of neutron and photon transport in PBRs. MCNP (Monte Carlo N-Particle) is such a code, whose generalized-geometry features and use of continuous-energy cross sections are increasingly making it the tool of choice for the analysis of nuclear reactors. Although the irregular packing of pebbles cannot be modeled exactly in the current version of MCNP (version 4B), an analysis of the HTR-10 has demonstrated the applicability of the code to PBRs.

The core of a light-water reactor is characterized by a fixed lattice of fuel assemblies. The application of Monte Carlo methods to the analysis of such a geometry is time consuming but straightforward. By contrast, the pebble-bed core consists of an irregular arrangement of fuel spheres, whose position and composition is constantly changing in time. This complicates the neutronic design of such a reactor, since this is based on an equilibrium fuel composition in the core. An MCNP-based fuel management and burnup capability is not currently available for PBRs. However, a procedure has been implemented for extracting the required compositions from VSOP and generating the corresponding MCNP material cards.

This hybrid approach to the modeling of PBRs provides the reactor analyst with a powerful design tool, combining the sophisticated fuel management capability of VSOP with the accuracy of MCNP. Monte Carlo methods are particularly useful for determining the reactivity worths of the control rods and shutdown absorbers in the graphite side reflector (which otherwise must be calculated using special  $S_N$  codes), and MCNP is also suitable for shielding and heat deposition calculations. An MCNP/VSOP model of the PBMR has been developed to demonstrate the method.

### 3.2.1 HTR-10 Physics Benchmark

The HTR-10 is a small (10 MW) pebble-bed test reactor under construction in China. Figure 3-16 shows a cross section of the reactor and its basic design specifications.

Being the latest PBR to be built, the IAEA has sponsored a physics benchmark problem of the HTR-10 initial core as part of its Coordinated Research Program titled "Evaluation of High Temperature Gas Cooled Reactor Performance." The physics benchmark consists of three problems, designated B1, B2 (with three temperature-dependent subcases B21, B22 and B23) which require the calculation of the effective multiplication constant ( $k_{eff}$ ) for several core configurations:

- a) **Problem B1.** Predict the initial cold critical loading ( $k_{eff} = 1.0$ ), either in terms of the number of pebbles or the height of the pebble bed, with the control absorbers fully withdrawn. Assume a core temperature of 20°C and a helium coolant pressure of 3.0 MPa.
- b) **Problem B2.** Calculate the effective multiplication factor,  $k_{eff}$ , of the core filled completely to a height of 1.97 m under a helium pressure of 3.0 MPa and at the following core

temperatures: 20°C (**B21**), 120°C (**B22**) and 250°C (**B23**). Assume that all control absorbers are fully withdrawn.

- c) **Problem B3.** Calculate the total reactivity worth of the ten control rods at a core temperature of 20°C and a helium pressure of 3.0 MPa.

- **10 MW(t) pebble-bed reactor**
  - **core: 197 cm H « 180 cm D**
  - **graphite reflector: + 100 cm**
  - **~25,000 fuel/moderator balls**
  - **17% enriched  $\text{UO}_2$  TRISO fuel**
  - **10  $\text{B}_4\text{C}$  control rods**
  - **7 small absorber ball units**
  - **3 irradiation sites**
  - **20 helium coolant channels**
- 57% : 43% fuel/moderator pebble ratio in startup core**

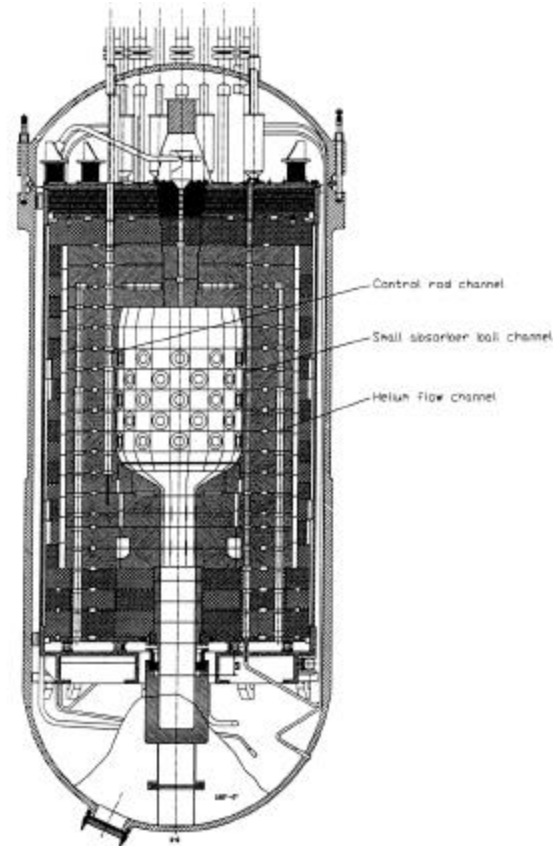


Figure 3-16. The HTR-10 Reactor.

These calculations were to be performed for a specified fuel-to-moderator pebble ratio of 57% to 43%. Since irregular packing of pebbles cannot be modeled using MCNP4B, the pebble-bed core must be idealized as a regular lattice of spherical pebbles. However, the specification of a 57:43 fuel-to-moderator percent ratio for the initial core loading complicates the modeling of the core using the repeated geometry feature of MCNP. Regular lattices composed of equal-sized spheres, which are characterized by even coordination numbers, cannot be used to model an uneven fuel-to-moderator ratio while preserving the original geometry of the pebbles. Instead, the core zone was approximated using a body-centered cubic lattice with moderator pebbles of reduced diameter.

The results of the MCNP analysis performed at MIT are given in Table 3-2, while Tables 3-3 and 3-4 summarize the preliminary HTR-10 physics benchmark results reported by other participants. Both diffusion-code and MCNP results calculated by several international organizations are shown.

Table 3-2. MCNP Simulation Results

Case	Critical Height (h) / $k_{\text{eff}}$ (k)	Cross Sections	Comments
B1	h = 123.5 cm k = $1.00046 \pm 0.00093$	ENDF/B-VI	300 K
	h = 123.5 cm k = $1.00166 \pm 0.00087$	UTXS	$\Delta p_{\text{bias}} = 1.2$ mk; 300 K
B21	k = $1.12976 \pm 0.00086$ k = $1.13185 \pm 0.00087$ k = 1.13220	ENDF/B-VI UTXS <sup>†</sup> UTXS	300 K 300 K 293.15 K; polynomial fit <sup>‡</sup>
B22	k = 1.12790	UTXS	393.15 K; polynomial fit
B23	k = 1.12452	UTXS	523.15 K; polynomial fit
B3	k = $0.95172 \pm 0.00096$ k = $0.95376 \pm 0.00101$	ENDF/B-VI UTXS	$\Delta p_{\text{rods}} = 165.6$ mk; 300 K $\Delta p_{\text{rods}} = 165.0$ mk; 300 K

<sup>†</sup> University of Texas at Austin cross-section library.

<sup>‡</sup>  $k(T) = 1.15328 - 9.35208\text{E-}05 \cdot T + 7.36721\text{E-}08 \cdot T^2$ , (T in °K); error not calculated.

Table 3-3. Diffusion Code Benchmark Results

Case	China <sup>1</sup>	Indonesia/Japan <sup>2</sup>	Russia <sup>3</sup>	Comments
B1	125.81 cm	107.0 cm	179.6 cm	critical height
B21	1.1197	1.2193	1.0290	k-eff
B22	1.1104	1.1983	1.0112	k-eff
B23	1.0956	1.1748	0.9938	k-eff
B3	152.0 mk	—	146.6 mk	control worth

<sup>1</sup>VSOP; <sup>2</sup>DELIGHT/CITATION-1000VP; <sup>3</sup>WIMS-D4/JAR

Table 3-4. MCNP Benchmark Results

Case	China <sup>1</sup>	Russia <sup>2</sup>	USA <sup>3</sup>	Comments
B1	~137 cm	164.6 cm	123.5 cm	critical height
B21	—	$1.0364 \pm 0.0008$	$1.1319 \pm 0.0009$	k-eff
B22	—	$1.0198 \pm 0.0008$		k-eff
B23	—	$1.0005 \pm 0.0009$		k-eff
B3	—	167.1 mk	165.0 mk	control worth

<sup>1</sup>MCNP4A and ENDF/B-V; <sup>2</sup>MCNP4A and ENDF/B-VI; <sup>3</sup>MCNP4B and UTXS.

There is clearly large variation in the results. However, there is good agreement with the MIT calculations using MCNP4B in two instances: the INET (China) prediction for the initial critical height, and the OKBM (Russia) estimate for the total control-rod reactivity worth. A high-fidelity MCNP model of a fresh core is expected to predict criticality within 2-3 mk. It is for this reason that MCNP models are often used to benchmark other codes. However, such an accurate

model cannot be readily developed for the HTR-10 startup core because of the proposed 57:43 fuel-to-moderator pebble percent ratio.

The accuracy of the codes will be determined ultimately through a comparison of the predictions with measurements during the initial approach to critical and low-power physics commissioning tests at the HTR-10 facility. Participation in this international effort was a valuable experience, both as a means for validating MCNP and as a testing ground for modeling methods.

### 3.2.2 MCNP4B/VSOP94 Model of PBMR

The 265 MW Pebble Bed Modular Reactor (PBMR), which is being designed by the South African utility ESKOM, is the basis for the nuclear design of a modular pebble-bed reactor at MIT. A vertical cross-sectional view of the reactor is shown in Figure 3-17.

Access to some ESKOM engineering specifications and the VSOP model of the PBMR has facilitated the development of a detailed MCNP4B model of the reactor (Figure 3-18). The core is idealized using 57 burnup zones, which correspond to the pebble flow channels and layers of the VSOP model. The material composition in each zone was extracted from the VSOP database for the equilibrium fuel cycle. The ESKOM design of the control rods and KLAK (KLeine Absorber Kugeln = Small Absorber Spheres) system is proprietary. An independent design of these systems, partly based on HTR-10 reactor specifications, is under way at MIT (Figures 3-19 and 3-20).

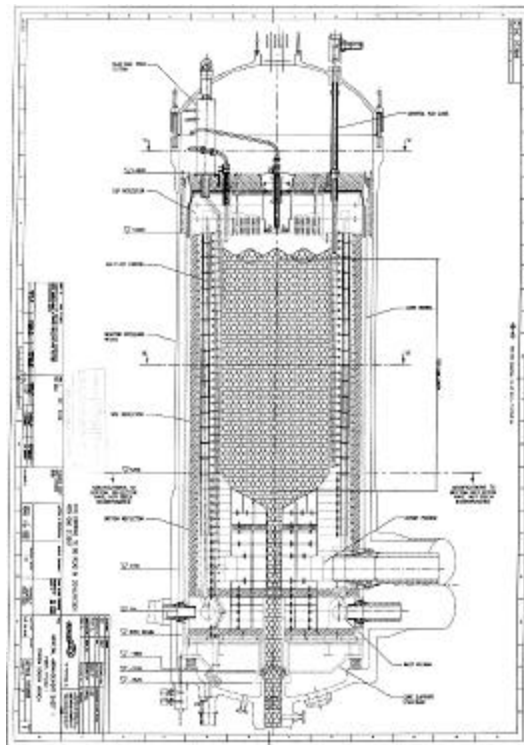


Figure 3-17. The ESKOM PBMR.



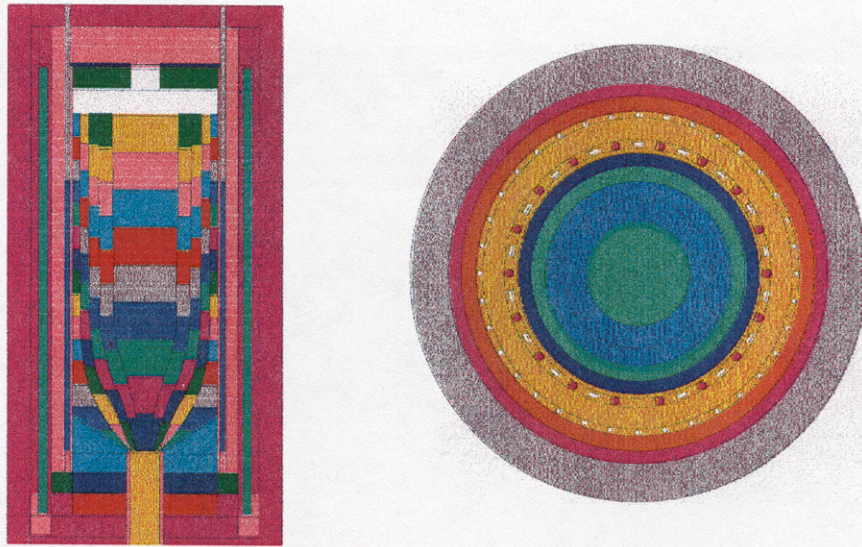


Figure 3-18. MCNP full-core model of PBMR.

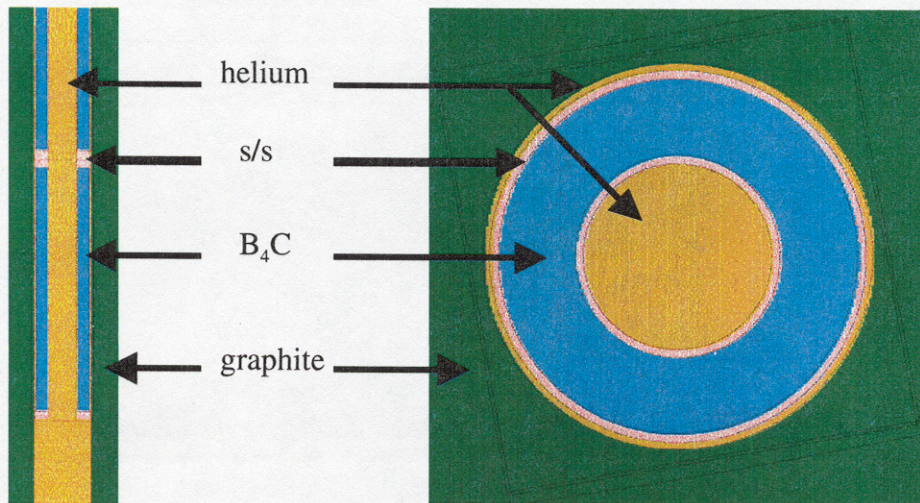


Figure 3-19. MCNP model of control site.

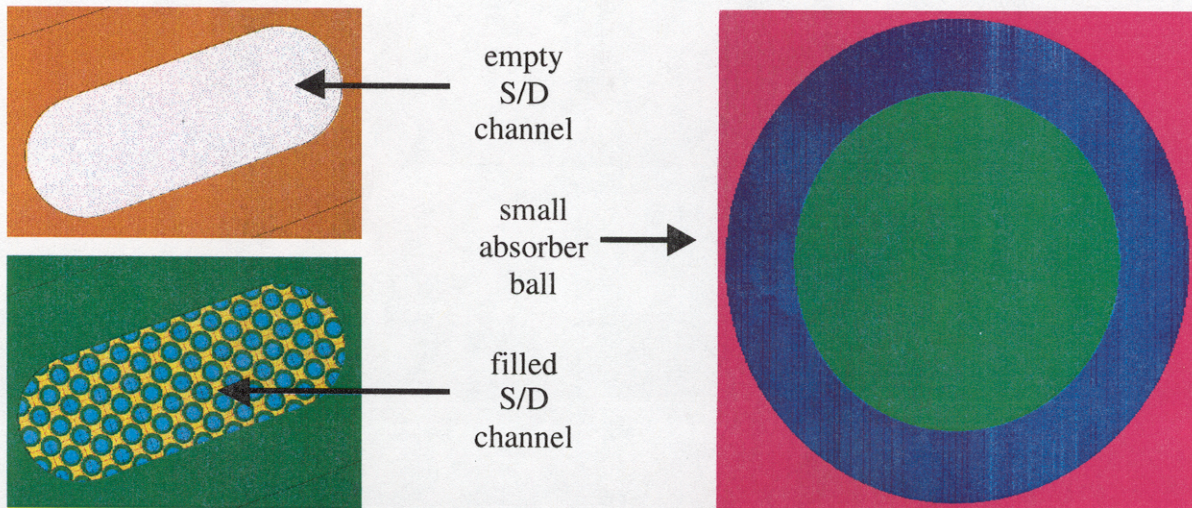


Figure 3-20. MCNP model of a shutdown (S/D) site.



Preliminary calculations have been performed to determine the flux and power distributions in the core. These are shown in Figures 3-21 through 3-23.

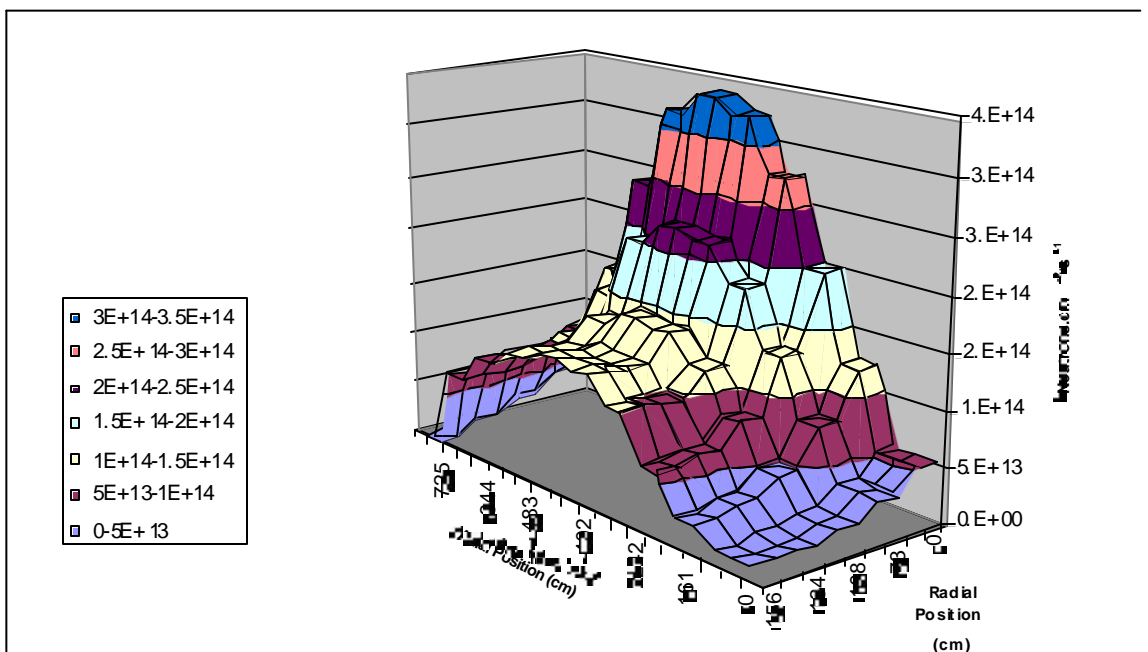


Figure 3-21. Thermal Neutron Flux in PBMR Equilibrium Core [Control Rods 1/4 Inserted ( $z = 201.25$  cm)].

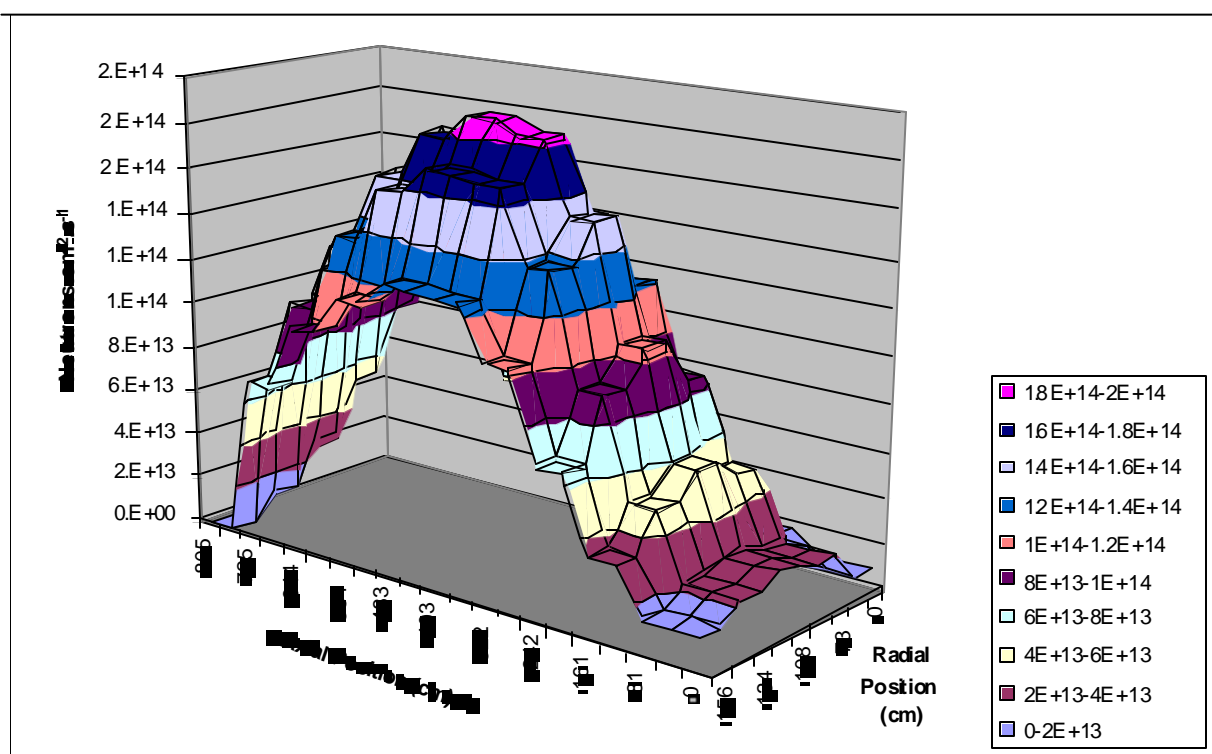


Figure 3-22. Fast Neutron Flux in PBMR Equilibrium Core [Control Rods 1/4 Inserted ( $z = 201.25$  cm)].



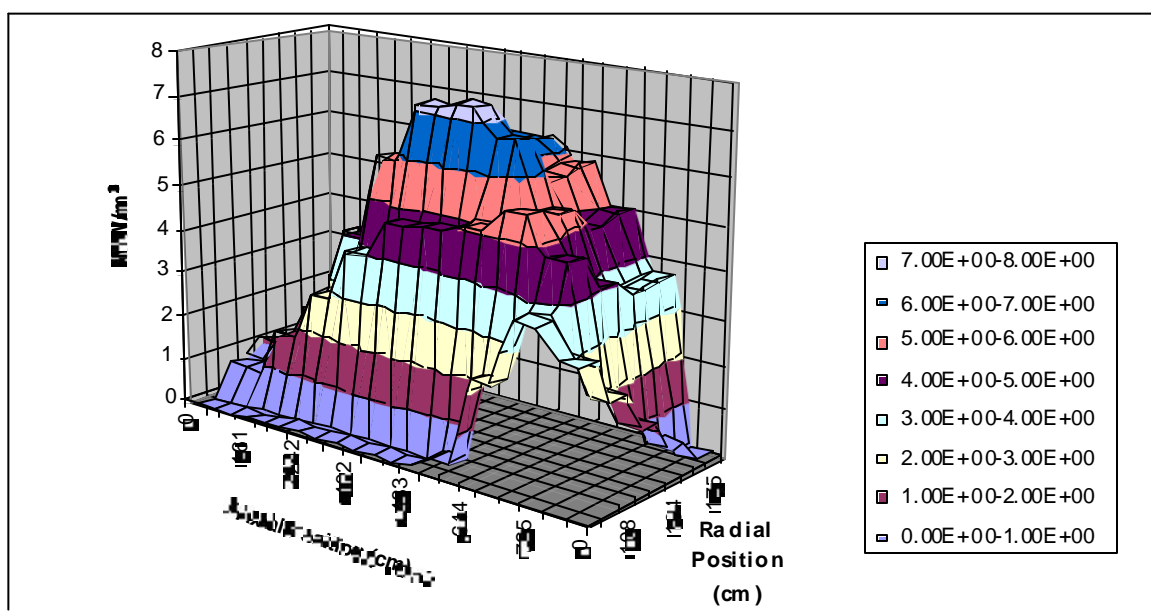


Figure 3-23. Power Density in PBMR Equilibrium Core [Control Rods 1/4 Inserted ( $z = 201.25$  cm)].

### 3.2.3 Nonproliferation<sup>a</sup>

The modular pebble-bed reactor is recognized for its simple design, thermodynamic efficiency, natural safety and environmental friendliness. The graphite pebbles with the embedded TRISO fuel kernels may serve as an excellent waste form for the direct disposal of spent fuel in a geological repository. In addition, as shown in Table 3-5, the isotopic composition of the high-burnup spent fuel offers a high level of proliferation resistance.

TABLE 3-5. Plutonium Composition in PBMR Irradiated Fuel<sup>†</sup>  
(100 MWd/kg HM)

Isotope	First Pass	Discharged
Pu-238	0.01 %	5.1 %
Pu-239	64.31	24.1
Pu-240	29.28	27.3
Pu-241	5.65	11.4
Pu-242	0.76	32.1

<sup>†</sup> Calculated using VSOP94.

The core contains a large inventory of fuel pebbles (approximately 295,000) which, in the normal mode of reactor operation, are recycled up to ten times through the core. An opportunity may thus arise to divert partially depleted fuel before it achieves the desired discharge burnup. The isotopic composition of such fuel would be more suitable for weapons production (see Table 3-5). The diversion of standard fuel does not pose a serious proliferation risk, because of the large number of pebbles which would have to be diverted (790,000 first-pass or 260,000

<sup>a</sup> Additional work on the proliferation resistance of the pebble bed gas reactor can be found in the companion URC project of the same name.



discharged fuel pebbles) and the duration of such an undetected diversion (7.5 or 2.6 years, respectively). However, dedicated plutonium production fuel pebbles, heavily loaded with natural or depleted uranium, require special consideration.

An MCNP4B analysis was performed, based on the PBMR reference core design, to determine the plutonium production capability using such special pebbles. A supercell model was used, which consisted of a single production pebble with a solid core of depleted  $\text{UO}_2$  surrounded by a critical spherical driver core with a graphite reflector (Figure 3-24). A body-centered cubic lattice was used to represent the packing of pebbles, and the driver fuel composition was taken from the VSOP equilibrium core model. Such a configuration has the advantage of ensuring that the neutron energy spectrum in the production cell, which comprises the production pebble in the center and an eighth of a driver pebble in each corner of the cube, is representative of the PBMR core.

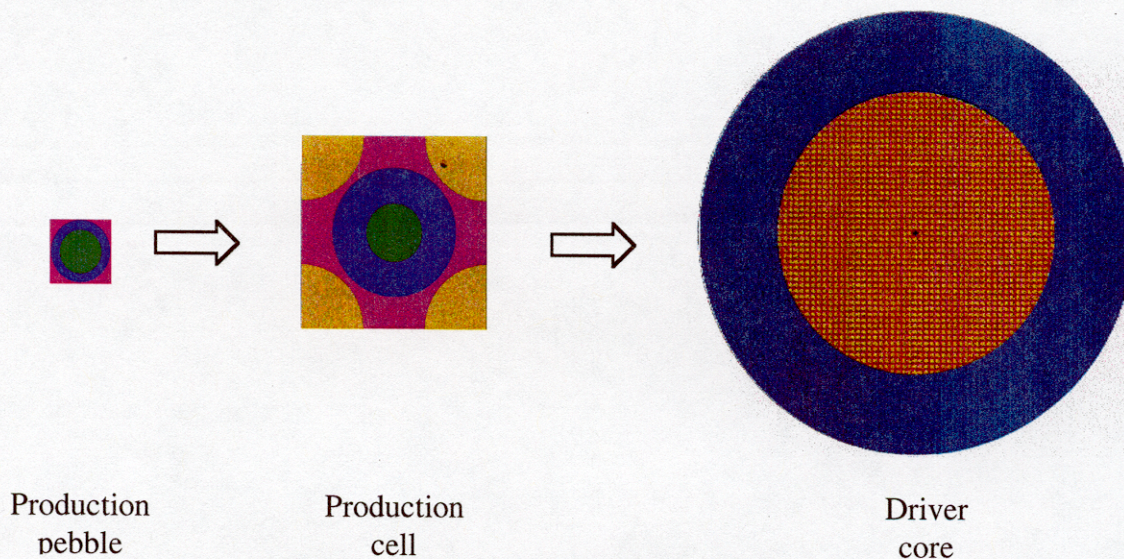


Figure 3-24. Supercell MCNP model.

The  $^{238}\text{U}$  capture rates in the two pebbles of the production cell were tallied, and their ratio based on four million neutron histories was found to be:

$$\frac{\text{special}}{\text{regular}} = \frac{52.0 \times 10^{12} \pm 6.62\%}{6.08 \times 10^{12} \pm 10.8\%} = 8.6 \pm 13\% \quad (3-18)$$

which is considerably less than the mass ratio  $362/8.28 = 43.7$  because of self-shielding.

The single-pass (~73 days) production rate of  $^{239}\text{Pu}$  in the reference PBMR design was estimated to be 0.015 g. Thus, the special pebble production rate scales up to  $0.015 \times 8.6 = 0.13$  g  $^{239}\text{Pu}$  per pass and, if 6.0 kg of  $^{239}\text{Pu}$  are taken to be one weapon's worth, this implies that  $6000/0.13 \approx 46,000$  special pebbles would have to be diverted. If such pebbles comprise 1% of the core inventory, it would take approximately 3.2 years to accumulate this quantity of material at the normal fuel-pebble removal rate of 164 per hour. However, because of the small amount of core excess reactivity, it is likely that the associated reduction in the fissile inventory would hinder the normal load-following operation of the reactor. A proper fuel management study of such a scenario is planned using VSOP.



*Future Work*

The following activities are planned for fiscal year 2000/2001:

- a) The implementation of the MCNP/VSOP link needs to be completed. Several issues remain to be resolved, including differences in the cross-section libraries used by the two codes and the way that impurities in graphite are handled by VSOP.
- b) The MCNP4B model of the PBMR can be improved considerably, although this task will require further input from ESKOM on the reactor structure and components. The control rods must be designed and analyzed properly to be of use for reactor dynamics and control studies.
- c) The modeling of a pebble-bed core with MCNP4B introduces several approximations whose significance must be determined. The effect of double heterogeneity on reactivity and neutron spectrum, as well as of the pebble-bed packing order on neutron streaming in voids, will be investigated.
- d) The applicability of MCNP4B, together with the ENDF-B/V and VI cross-section libraries, to pebble-bed reactors will be confirmed by benchmarking the code against the HTR-PROTEUS critical experiments. The accuracy of the MCNP model will be verified through comparison with VSOP predictions for the start-up core.

The investigation of fuel cycles is required to address issues that are vital to the successful introduction of pebble-bed reactors in the US. The safety, proliferation resistance and cost of competing fuel cycles (LEU, Th/LEU) and management strategies (multi-pass and single-pass with burnable poison) will be examined using the VSOP code. Comparisons will be made with the prismatic HTGR and current LEU fuel cycles, including the proposed Radkowsky Seed-and-Blanket PWR. An MIT/INEEL numerical benchmark should be performed for an equilibrium, reference HTGR core design to facilitate comparison of different code predictions.



## 4. Safety and Thermal Hydraulics

### 4.1 Power Conversion System Development

The goals of this task are: (1) the development of a steady state model for the plant, (2) to extend this model for transient behavior and to develop a plant simulator, (3) to use these models to establish individual component design parameters and to optimize the power conversion system design and (4) to examine issues related to working fluid choices. Figure 4-1 schematically illustrates the task plan and how the individual tasks interact.

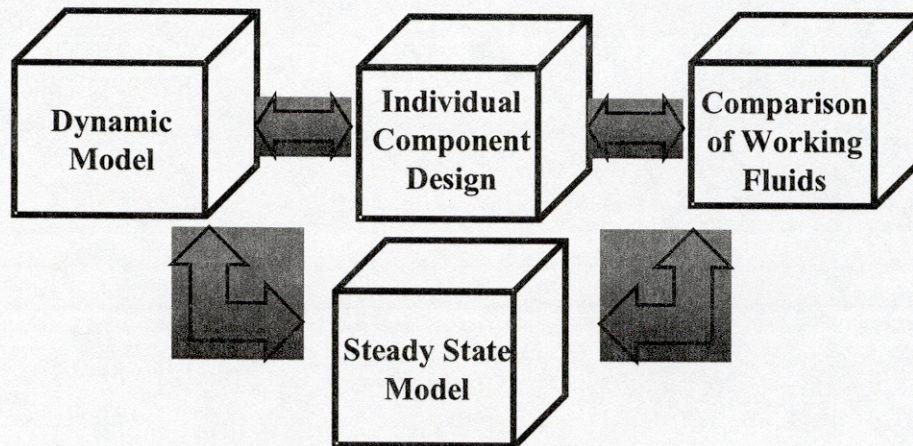


Figure 4-1. Schematic for power conversion system component interactions.

The economic viability of the overall plant depends heavily on the efficiency of the power conversion system. Moreover, unlike a conventional Rankine cycle, the efficiency of the Brayton cycle is highly sensitive to the design of individual components and their integration within the cycle. The efficiency of the Rankine cycle is relatively independent of the fraction of full power. The Brayton cycle, on the other hand, is extremely sensitive to component design during intermediate power operation. Lastly, the cost of the power conversion system hardware is extremely sensitive to the desired efficiency of individual components, in particular the heat exchangers. Because of this complex interaction, it is not enough that an individual component be economic and efficient by itself. The efficiency of the power conversion system and cost depend on each component being fully integrated into the system. As an example, heat exchanger effectiveness can be specified within reasonable limits between 0.9 and 0.95 (or even higher). However, the size of the higher effectiveness unit will be approximately double that of the 0.9 unit. This will be reflected in the cost. Another major impact on system cost will be the choice of working fluid. The current design calls for helium as the working fluid. However, there are those who are concerned about uncertainty in the cost of helium turbomachinery. The concern is that there may be extensive development costs associated with untried helium components and that these costs will negate the other advantages of helium. Air, on the other hand, has an extensive experience base for open cycle gas turbine systems. Thus, a comparison of the two working fluids is an important component of the project.



For the above reasons, the design of the power conversion system requires the development of an accurate plant model for both steady state and transient analysis. Additionally, a comparison of the two working fluids, helium and air, needs to be done. During this reporting period, progress has been made in both areas.

#### 4.1.1 Plant Description

Table 4-1 shows the basic plant parameters. Figure 4-2 shows a schematic of the basic plant layout. The core thermal output is nominally 250 MW. The core is of the pebble bed design in which fuel, in the form of “pebbles” pass continuously through the core during operation. The fissile material is contained in microspheres, approximately 11,000 per pebble, in which a series of pyrocarbon and silicon carbide layers surround a fuel kernel. These layers act as both the pressure boundary and as the containment for fission products. The core gas exit temperature is 850°C. The power conversion system consists of a two shaft, recuperated and intercooled Brayton cycle. The power conversion system is interfaced with the primary helium system via an intermediate heat exchanger. While most other gas reactor designs use a direct cycle, the current design uses an indirect cycle. The indirect cycle has the advantages of (1) easier maintenance. In principal the power conversion will not be radioactive, and (2) provides a barrier to water ingress into the primary system. These advantages are achieved at the cost of slightly lower thermal efficiency and increased complexity. The power turbine is synchronized to the electric grid at 3600 RPM. Power conversion system control is achieved via bypass control for fast transients and volume control for load following and slow transients. Reactivity control is achieved via control rods located outside the core in the reflector region. Primary system mass flow rate is controlled by a variable-speed helium circulator.

Table 4-1. MPBR Plant Parameters

Thermal Power	250 MW
Core Height	0.0 m
Core Diameter	3.0 m
Pressure Vessel Height	16 m
Pressure Vessel Radius	5.6 m
Number of Fuel Pebbles	360,000
Microspheres/Fuel Pebble	11,000
Fuel	UCO or UO <sub>2</sub>
Fuel Pebble Diameter	60 mm
Fuel Pebble enrichment	8%
Uranium Mass/Fuel Pebble	7 g
Coolant	Helium
Helium mass flow rate	120 kg/s (100% power)
Helium entry/exit temperatures	450°C/850°C
Helium pressure	80 bar
Mean Power Density	3.54 MW/m <sup>3</sup>
Number of Control Rods	6
Number of Absorber Ball Systems	18

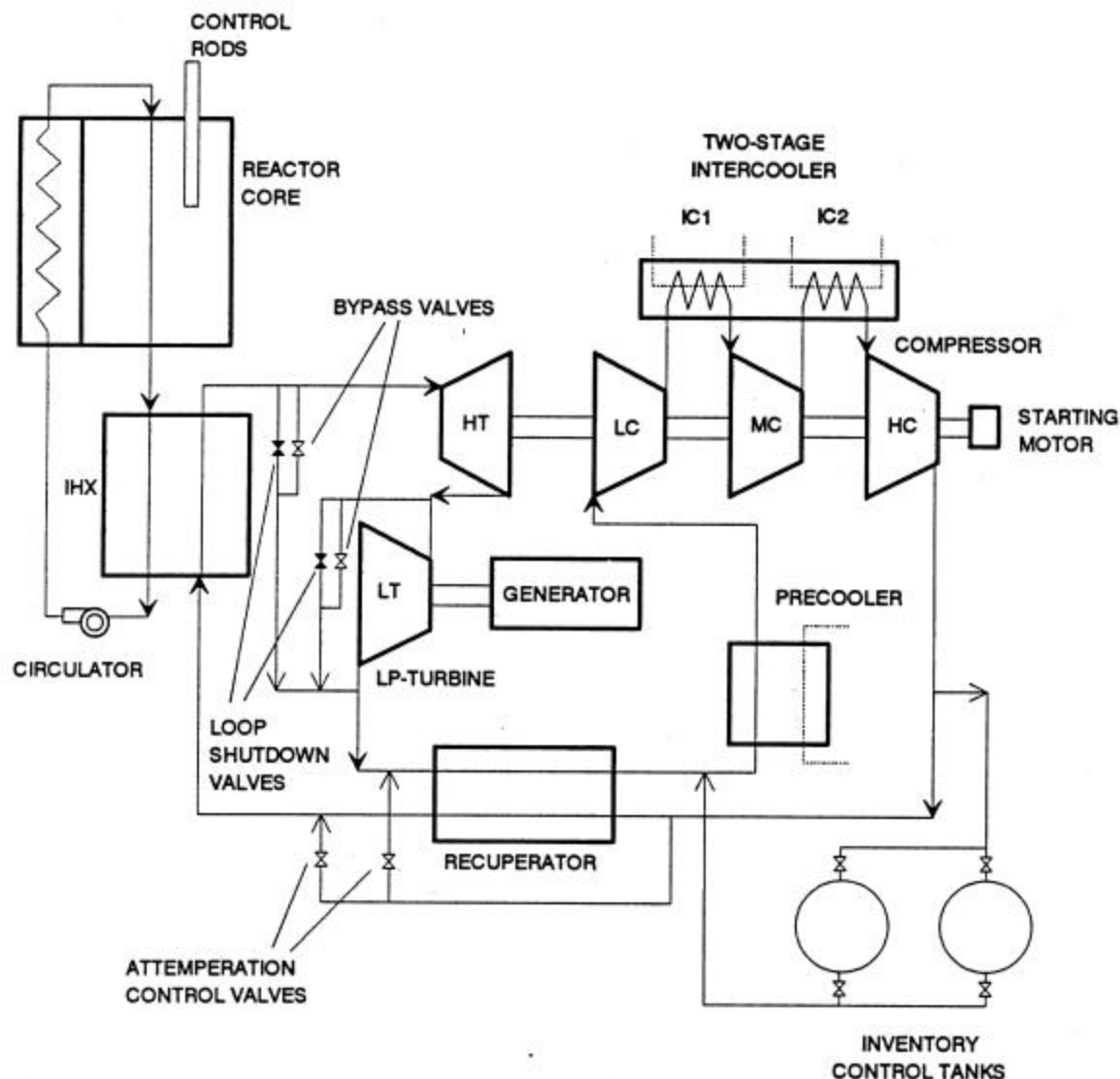


Figure 4-2. MPBR and power conversion system schematic.

#### 4.1.2 Power Conversion System Model Development

During this reporting period, the major focus has been in developing a detailed description of the transient model of the power conversion system. At the beginning of the project, we thought that we could build on previous work in this effort. However, the two sources of previous transient models, previous work done at MIT and a model developed at ORNL, either were not available or proved to be poorly developed. For these reasons, it was decided to begin with a clean sheet of paper and to develop a model which would best serve the needs of the project. A detailed specification of the requirements for our model is still in process. However, the initial specifications and design of the system have been completed. Figure 4-3 shows a schematic of the basic building blocks of the system.



Figure 4-2 shows a schematic of the overall system. As was discussed earlier, the power conversion system will consist of a two-shaft, recuperated and intercooled system. The high temperature turbine drives three compressors at 10,000 rpm. A starting motor is used on this shaft for startup. The low-pressure turbine drives the generator, which is synchronized to the power grid and rotates at 3600 rpm. An intermediate heat exchanger transfers heat from the primary helium circuit to the power conversion system. The purpose of the intermediate heat exchanger is to prevent contamination of the power conversion system. This, in principal, will allow for easier maintenance of the power conversion system. The primary helium is circulated through the core via a variable speed circulator.

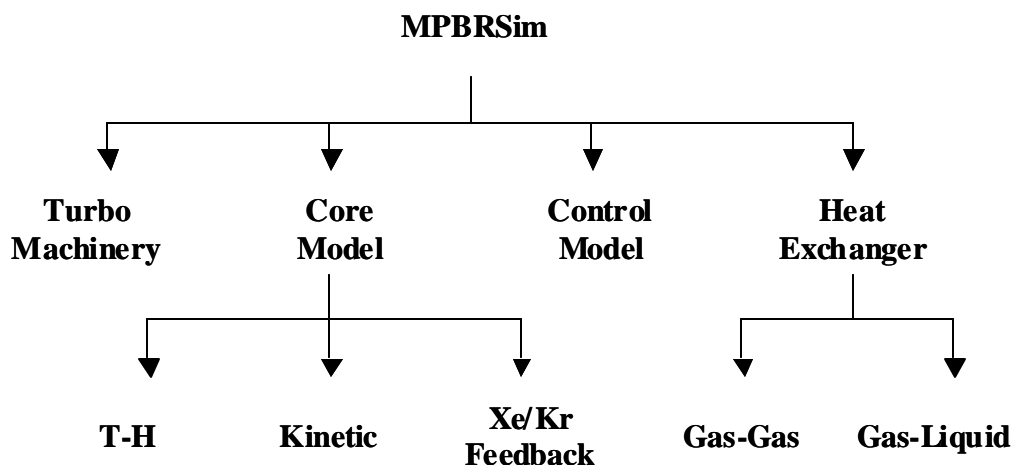


Figure 4-3. Schematic of the power conversion system simulator.

Power level control for the system is achieved using one or more of the following methods in combination:

1. Control rod motion
2. Primary circulator speed
3. Bypass control in the power conversion system, which can shunt flow around either the high-pressure or the low-pressure turbine.
4. Inventory control in the power conversion system.

The control system must be capable of both normal startup and shutdown of the plant as well as power maneuvers during normal load following and transient control during upset conditions. The control system will be designed to use electrical demand as the primary control variable during normal operation. The design ramp rate for the system will be 10%/min.

The transient system model is being written using the ACSL system simulation language. ACSL is an industry standard simulation tool. The development path has been to first assemble a model, which contains very simple models for each component. After this has been accomplished, the transient system model will be assembled using the ACSL language. The system will then be tested at steady state. Once stability has been obtained, detailed component models will be developed. Finally, the transient control model will be developed.

Once the transient model has been developed, the model will be used to optimize individual components to produce a final system design.

During this reporting period the following progress has been made:

1. The overall transient model components have been assembled. Simple models for each component have been developed.
2. The transient model has been verified stable at steady state.
3. Detailed models for the reactor and the heat exchangers have been developed. The core model has been verified against closed form solutions.

### *Reactor Model*

A detailed initial core thermal-hydraulic and neutronics model has been developed. For thermal hydraulic purposes, the core is divided into 5 equal-volume radial rings in the fueled region, 1 radial ring in the central, unfueled region, and 1 radial ring in the reflector. The core is sectioned into 12 axial slices. The fueled region is treated as being homogeneous for purposes of calculating an average density. Helium conduction and heat loss from the reactor vessel are assumed to be negligible. Pebble bed effective thermal conductivity takes into account both conduction and radiation (see References 22, 23, and 24).

The core neutronics is modeled using a one-group point kinetics treatment. Both Xenon reactivity effects and the effect of temperature on reactivity (Doppler) are modeled. Xenon reactivity effects are treated using a simplified production and removal scheme illustrated in Figure 4-4. Future development of the model will include a six-group point kinetics treatment to represent more accurately the temperature effects on reactivity.

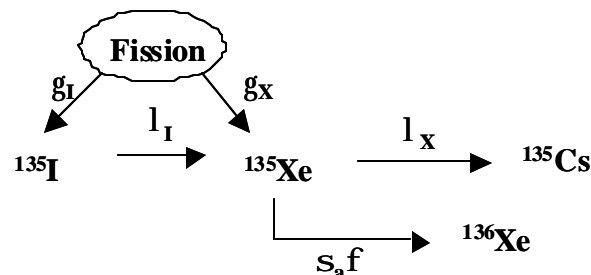


Figure 4-4. Xenon production and removal schematic.

Figure 4-5 shows the calculated  $Xe^{135}$  transient, which occurs during shutdown. The xenon concentration builds up initially due to decay of the  $I^{135}$  parent and then decreases as it decays. As the  $I^{135}$  decays to xenon there comes a point where the xenon concentration peaks—at about 10.5 hours, after which, the Xenon concentration decreases.

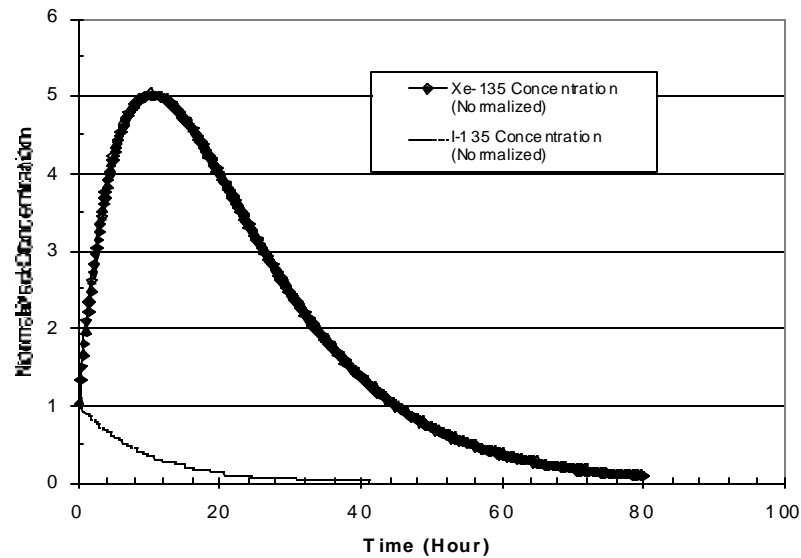


Figure 4-5. Shutdown Xenon transient.

Figure 4-6 shows the response of the transient core model to the insertion of  $\pm 0.22\%$  reactivity. The closed form calculation and the model response are very close.

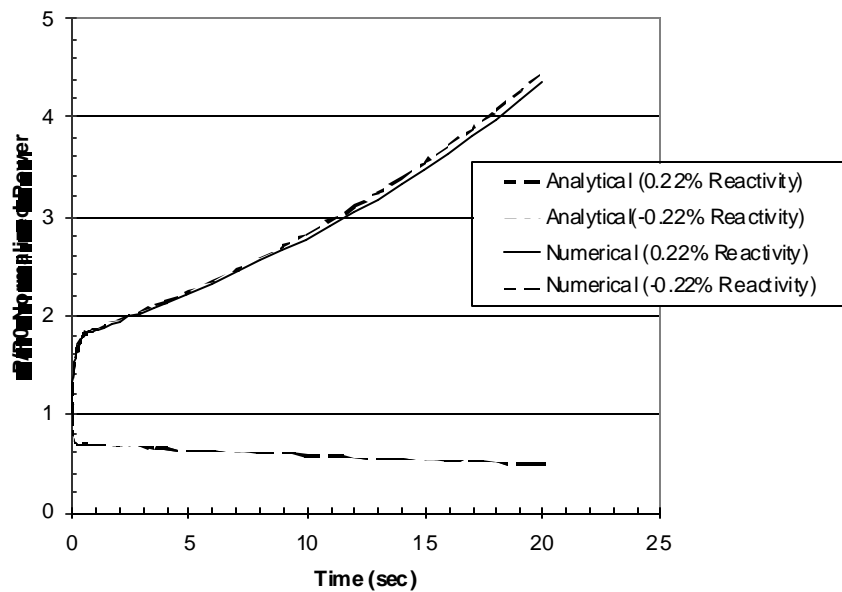


Figure 4-6. Verification of transient core model for reactivity addition.

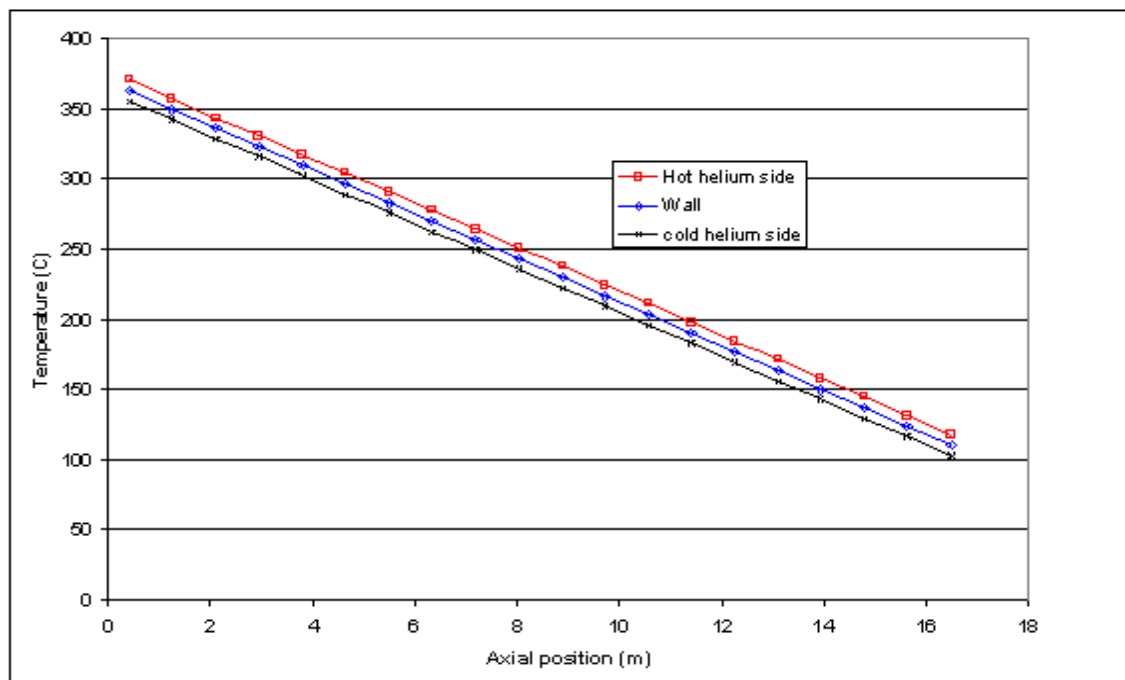


Figure 4-7 Recuperator steady state temperature distribution.

#### *Transient Heat Exchanger Model*

The transient heat exchanger model currently accommodates only counter flow designs. This is the design that will likely be used for all of the heat exchangers in the power conversion system. However, the model can be changed to include other designs if needed. The model takes into account the metal mass of the heat exchanger. The heat exchanger can be divided into an arbitrary number of segments. Figure 4-7 and 4-8 show a recuperator steady state temperature distribution and transient response to a step temperature increase of 200°C at hot inlet side, respectively. The steady state result agrees with the closed form calculation result.

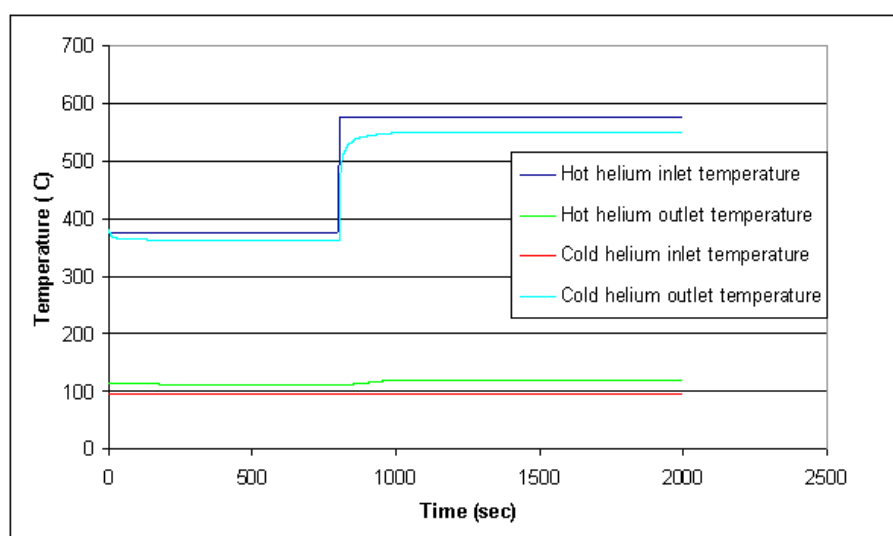


Figure 4-8 Recuperator transient response to a step temperature increase of 200 °C at hot helium inlet side.

### 4.1.3 Working Fluid Comparison

As was discussed earlier, the choice of working fluid will have a very significant effect of what the system actually looks like. Heat exchanger sizes, turbine and compressor configuration all depend on the choice of working fluid. Hence, the overall economics of the system will be influenced by the choice of working fluid. Figure 4-9 illustrates the interaction of the choice of working fluid with the overall design.

The MPBR reference design calls for helium as the working fluid. However, the largest experience with gas cooled systems, open cycle gas turbine technology, uses air as the working fluid. This large experience base would, in principal, allow an air working fluid system to be brought to market with less R&D effort. For this reason, it was decided to make a comparison of the two fluid options. The details of this comparison have been reported in a project funded SM thesis.<sup>25</sup> Here we will only provide a summary.

For the comparison exercise, three systems were chosen: (1) the air open-cycle system, (2) the air closed-cycle system and (3) the helium closed-cycle system. In point of fact, while the experience base for the air open cycle is the largest, this cycle is unsuitable for use in the MPBR due to the risk of contamination release should a leak develop in the intermediate heat exchanger. The proper head-to-head comparison is between the two closed cycles. However, the air open cycle has been kept as part of the comparison as a reference.

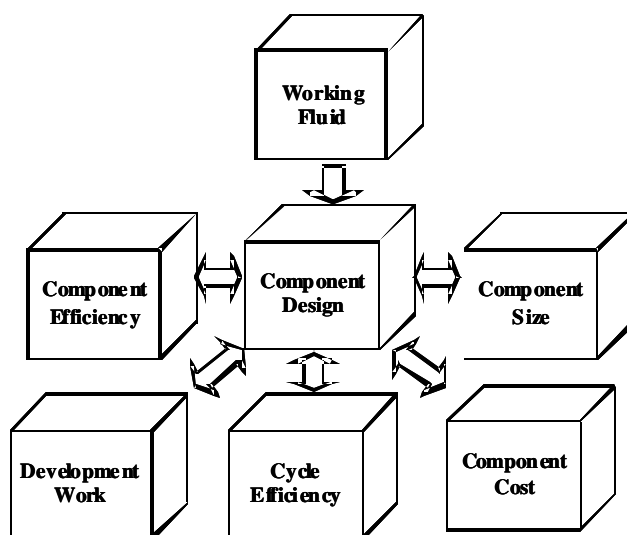


Figure 4-9. Interrelationships between design choices and working fluid.

The comparison considered a number of factors but the major ones were: (1) an estimate of the required development to bring each system to market, (2) system efficiency, and (3) component cost and size. Size was an important factor due to a requirement that the overall MPBR system components be shippable via truck or rail to the site in semi-assembled form.

#### *Industrial Experience Comparison*

As was discussed above, the air open cycle has the largest industrial experience base. When comparing the closed cycle experience for air and helium the two experience bases are comparable in size. The air closed-system experience is much more limited than for the open cycle. The first air closed system was built in 1939 in Switzerland.<sup>26</sup> Approximately 20 plants were built in Europe following World War II with power outputs up to 20 MWe.<sup>27</sup> Helium experience is limited but still significant. The largest helium system was built in Oberhausen Germany with an output of 50 MWe.<sup>28</sup> In addition, as part of the AVR development program in Germany, several large helium circulators have been built and tested in experimental loops. Based on these experiences we conclude that both the air and helium closed cycle systems would require approximately the same development effort. However, with respect to the helium system, it was judged that the technology was mature to the point where systems in the size range of the MPBR could be built. This judgment was further confirmed in discussions with industry.<sup>29</sup>

### *System Efficiency Comparison*

System efficiencies were compared for each system with the single constraint that reactor inlet gas temperature was fixed at 445°C. This is the maximum allowable temperature for a pressure vessel fabricated from 9Cr-1-MoV steel in accordance with ASME Class 2&3 Pressure Vessel Code Case N-47. All other design parameters (pressure ratio, number of turbine stages, etc.) were optimized for the working fluid in question. Table 4-2 presents the results of this comparison.

Table 4-2. Thermodynamic Comparison Results

	Helium	Air Closed	Air Open
Pressure Ratio	3.7	7.4	7.3
Busbar Efficiency	44.8%	46.0%	46.8%
Turbine $T_{in}$ (°C)	828	828	828

The air cycles show a slightly higher efficiency than the helium cycle. However, the difference is only about 1% between the two closed systems.

### *Size Comparison*

Table 4-3 shows a comparison of approximate component volumes for the three systems. The physical properties of helium result in a larger turbine/compressor set. However, this is more than balanced by the very large heat exchangers required for the air systems. This is due primarily to the larger specific heat and thermal conductivity of helium. This factor dominates the system design and gives the advantage to helium. In fact, the large volumes required for the heat exchangers in the air system would not be truck transportable.

### *Overall Comparison*

Based on the total comparison results we conclude that helium is the best choice as working fluid. Moreover, we conclude that the existing helium component experience base is applicable for extrapolation to MPBR conditions.



Table 4-3. Component Volume (m<sup>3</sup>) Comparison

	Helium	Air Closed	Air Open
IHX	17	86	260
HP Turbine	0.27	0.06	2.2
LP Turbine	0.58	0.22	13
LP Compressor	0.35	0.13	2.7
Recuperator*	13	61	180
Precooler*	50	97	----
Intercooler #1*	41	80	180
Intercooler #2*	41	80	180
Total Volume	160	400	820

\*Assumes air cooling. If water cooling is used volumes would be reduced considerably.

### *Industry Collaboration*

During this reporting period, two important industrial collaborations were established. A collaboration has been initiated with General Atomics (GA) in the area of transient model and simulator development. GA developed a simulator and transient model for the prismatic core configuration. Their power conversion system is a direct cycle, single shaft system. However, their transient simulator model has a number of similarities with our model. Additionally, their experience in developing their model would be of significant use in our development effort. GA has agreed to support us in this development effort by providing manpower and on-site (at GA) assistance with our effort.

In the area of turbo-machinery and heat exchanger design, we have entered a collaboration with Northern Research and Engineering Company (NREC). NREC is a major player in the design of compact heat exchangers and turbo-machinery for gas applications. NREC was one of the bidders for the development contract with ESKOM for their pebble bed design.

## **4.2 Safety Analysis**

This effort started in February in an attempt to identify important safety issues affecting past high temperature gas nuclear reactors. A student was assigned to review past NRC Safety Evaluation Reports of General Atomics 330 MWe prismatic reactor license application and other reports on severe accident analyses for these types of reactors. The important concerns are related to fuel reliability, air and water ingress accidents, helium leakage and the need for a containment. In the design course of the spring of 1999 students performed an assessment of the need for a decay heat removal system in the event of a loss of coolant accident or loss of cooling function. This analysis was simplistic but did show that the peak fuel temperature would not exceed the design limit of 1600°C.

In this reporting period, MIT reanalyzed the loss of coolant accident. They used a more accurate Heating 7 but still very conservative (no convection cooling of the reactor cavity) model of the reactor, the concrete reactor cavity and the earth which is assumed to be the ultimate heat sink. The results shown in Figure 4-7 indicate that the peak fuel temperature reaches 1557°C which is below the design target level, however the temperature of the reactor vessel and concrete in the reactor cavity are high enough to require some cavity cooling for structural integrity reasons.

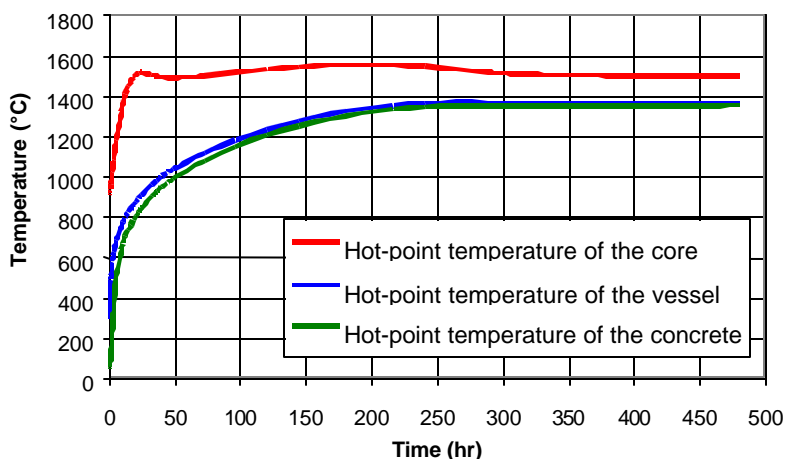


Figure 4-10. Loss of coolant accident results using Heating 7.

Another series of independent calculations were performed assuming convection of air in the reactor cavity to assess the impact of convection at various air velocities expressed in meters/sec. The results of this analysis are shown on Figure 4-11. Within the limits of this sensitivity analysis, significant reductions in vessel and concrete temperatures are observed. The maximum temperatures calculated for the vessel and concrete in the cavity are in the range of 525°C and 425°C respectively. These are still high for materials and further analysis is required to demonstrate total passivity. Future work will include an assessment of the type of passive reactor cooling system needed to keep the vessel and concrete temperatures within safety limits.

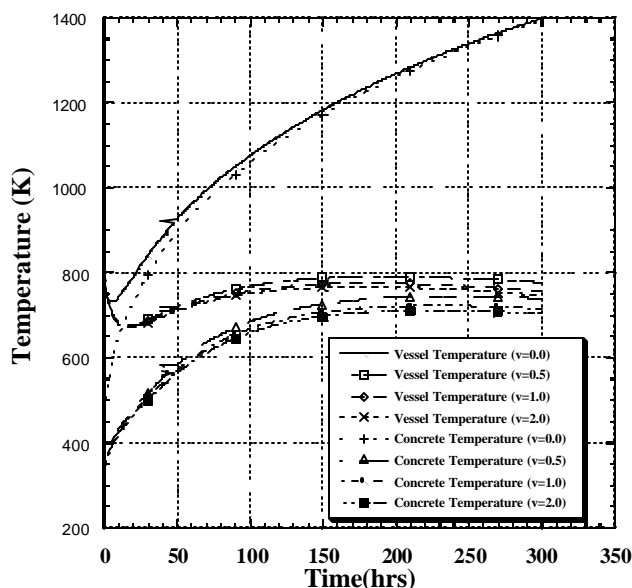


Figure 4-11. Temperature changes including convection.

One of the other important issues for a gas reactor is its ability to deal with an air ingress event. During such an event, the helium in the coolant circuit depressurizes as a result of a leak or break in the primary circuit. Air is then be able to stream through the core according to free natural convection leading to graphite oxidation, which results in an exothermic reaction. Experiments in Japan have demonstrated that such an exchange flow between air and helium

can occur even with only one break in the system because of flow stratification at the break. Thus, previous claims that such an event could only occur when two breaks occurred in the system to produce a "chimney" were in error. Therefore, our thermal hydraulic work has been focused on studying this potential accident scenario. We have reviewed the existing data on graphite oxidation and begun to evaluate the air ingress invent analytically. Integrated modeling using ATHENA and MELCOR will be performed next year.

Oxidation processes of graphite are classically described by three different temperature regimes as shown in Fig. 4-12. At the low temperatures in Regime 1, the reaction rate is controlled by oxygen reaction with active sites within the graphite. The percentages of sites within graphites that are reactive are very low and graphites are in general quite porous. Oxygen, or the oxidizing gas, will have the opportunity to diffuse sufficient distances into the material. Oxidation rates can therefore be expressed as a bulk rate based upon mass, e.g., g/(g-s). As temperature is increased into Regime 2 more sites within the graphite become active. Oxygen diffusing within the pores of the graphite is consumed at near-surface locations in the graphite. Oxygen supply in the gaseous boundary layer controls the reaction in Regime III at the highest temperature. Reaction with the graphite occurs at the outer surface of the graphite and rates are therefore expressed based upon the surface in terms of g/(cm<sup>2</sup>-s). In addition to these surface effect, the ability to get air into the reactor and to graphite must also be considered.

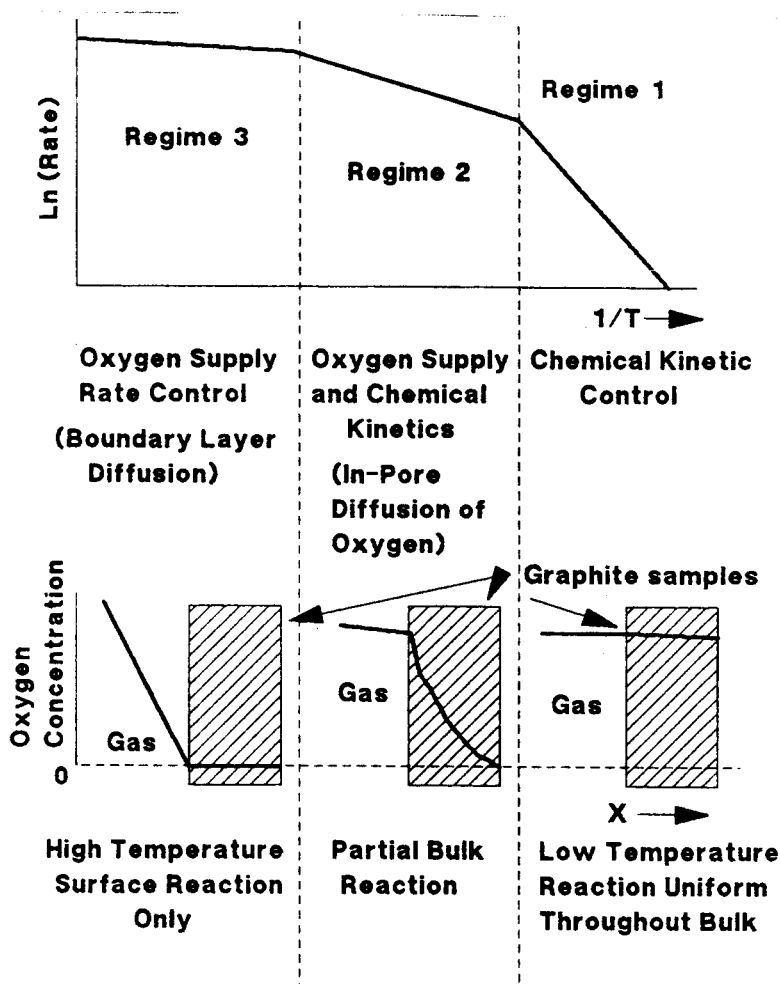


Figure 4-12. Classical depiction of three temperature regimes, showing the controlling mechanisms for reaction of graphite with air (or other oxidizing gas).

There has been a wealth of data generated on graphite oxidation in air. Wichner and Ball have made a comprehensive review of this literature (Ref. 30). They have summarized data to be use for modeling accidents in gas-cooled graphite reactors. They have addressed many of the variables influencing oxidation rates at low temperatures in Zone I. These include influences from manufacturing processes, impurities, oxygen partial pressures, extent of burnoff, neutron irradiation effects, and redeposited carbon. Transition temperatures from one zone to another are somewhat indiscrete and influenced by several of the previous variables. Wichner and Ball have simplified this process somewhat and represent oxidation rates by only two regimes, i.e., Zone I and Zone III. They have incorporated the effect of many of the above mentioned effects into their reaction equations for these two regimes.

Providing common units for reaction rates over the entire temperature spectrum is needed from a modeling standpoint. Calculations shown in Figures 4-13 and 4-14 indicate that conversions that are required to go from surface-based reaction rates to mass-based reaction rates. The calculations are made using the volume to surface ratios of the spherical geometry for the pebbles. The initial pebble diameter is 6.0 cm and then decreases with burn-off from the outer surface. This condition applies to Zone III where reaction occurs primarily at the outer surface. Figure 4-12 shows the decrease in pebble diameter as mass is reacted from the outer surface. It shows that the diameter of the pebble decreases by less than one cm with a 20 percent mass burn-off. This would represent less than the 5-mm fuel free zone on the outer perimeter of the pebble. Conversion from an area-base rate,  $R^A$ , to a mass-based rate,  $R^M$ , can be made using the surface to volume correlation for a sphere and  $1.7 \text{ g/cm}^3$  as the density for graphite. Figure 4-14 shows how the conversion factor changes as the pebble diameter decreases with burn-off. The plot is relatively flat and shows only minor changes with 20 to 40 burn-off.

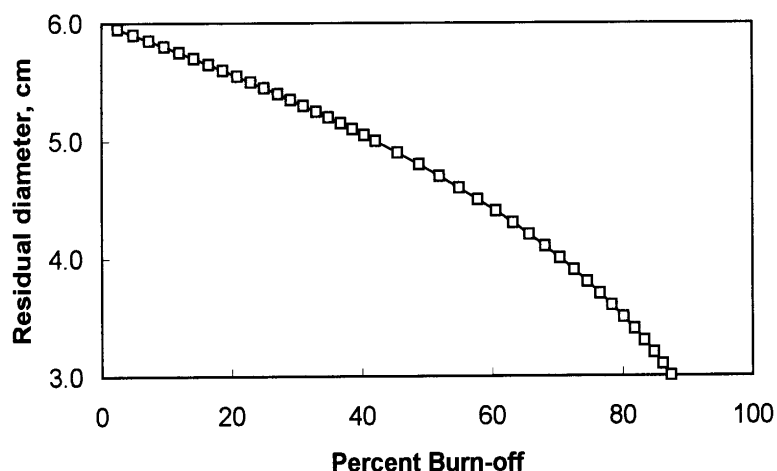


Figure 4-13. Diametrical change of a 6.0 cm diameter pebble as material mass is reacted or burned from the outer surface of the pebble.

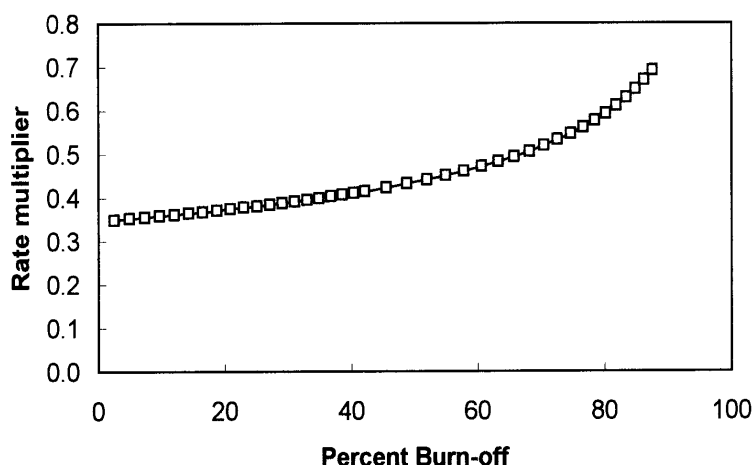


Figure 4-14. Conversion factor to change from a surface-based rate, e.g.,  $\text{g}/(\text{cm}^2\text{-s})$ , to a mass-based rate,  $(\text{g/g-s})$ , as material is reacted from the surface of a 6.0-cm diameter graphite pebble.

In addition, we have begun to set up a scoping model for the air ingress event using RELAP5/ATHENA and control variables to characterize the process. The air ingress is postulated to be induced from the containment tank after a depressurization accident takes place. Our future activities are focused on:

- evaluating the graphite oxidation database to establish the best data to use in the evaluation,
- performing experiments on graphite oxidation using techniques developed at the INEEL to measure such behavior
- evaluating the effect of air circulation in the vessel and transport across the non-condensable carbon monoxide/carbon dioxide layer that is formed on the overall oxidation,
- completing the RELAP5/ATHENA thermal hydraulic model to account for all of the important mass transport effects
- developing a MELCOR model to evaluate the same problem and thus have a benchmark for RELAP5/ATHENA



## **5.0 Other Activities**

### **5.1 Economics**

The cost estimates prepared by the design class were reviewed to show that the costs estimated could be duplicated. Additional reviews are underway to refine these cost estimates further to provide a better basis for pebble bed costs as compared to the prismatic reactor used as the basis. In addition, a preliminary cost estimate assuming that the plant could be built as a “merchant” or independent power producer plant. This cost estimate incorporates an aggressive depreciation schedule with restructured financing once the unit becomes commercial. It also assumes a market based price upon which to judge competitiveness and cost targets.

In preparation for a proposal to build a “reactor research facility”, the cost estimates prepared for the nth unit were reviewed to determine the rough cost estimate for the first unit in a demonstration type machine. These estimates also require refining but do provide a general idea of the level of funding that would be required. This information will be used to develop a business model and partnership arrangement between the government and the private sector for its eventual construction.

### **5.2 Regulatory Licensing Strategy**

In order for this plant to be licensed in a reasonable period of time since it is a technology that is non-traditional from the NRC perspective, it is important to develop a licensing process that can accommodate new technologies. A “license-by-test” strategy has been prepared that is based on risk informed and performance based approaches. This strategy is based on public health and safety goals using a process similar to that being applied in South Africa in the licensing of the ESKOM pebble bed plant. An outline of that process has been developed and is being reviewed with the NRC. Chairman Meserve of the NRC offered to work with the South African licensing authorities on a risk informed performance based process.

## 6.0 Conclusions

In general, the project has made significant progress during this year. The overall progress is summarized as follows:

### Fuel Performance Model Development

- We have developed four conceptual models for fuel particle failures that are currently being evaluated by a series of ABAQUS analyses. Analytical fits to the results are being performed over a range of important parameters using statistical/factorial tools. The fits will be used in a Monte Carlo fuel performance code, which is under development. This work will continue next year focusing on using the results to establish operational regimes (or fuel maps) for the key parameters
- The new fuel failure model yields more realistic predictions of reliability. A fracture mechanics based failure model has been developed and implemented.
- Thermal and chemistry models are taking shape with the diffusion experiments ready to run. Chemistry modeling will be accelerated next year.
- Next year we will begin the task on integrating all of these submodels into the overall fuel performance code.

### Thermal Hydraulics and Reactor Safety

- A balance of plant, steady-state thermal hydraulics model has been developed which represents all major components of a MPBR. Component models are being refined to accurately reflect transient performance. Individual component models are being developed. Reactor and heat exchanger models have been developed and verified.
- The initial transient model has been developed.
- A comparison between air and helium for use in the energy-conversion cycle of the MPBR was completed and the results suggest that helium is the best choice.
- Industry collaborations have been established with General Atomics and Northern Research and Engineering.
- Safety issues associated with air ingress are being evaluated with more analysis and experiments on air/graphite interactions planned for next year.
- Post shutdown, reactor heat removal characteristics are being evaluated by the Heating-7 code and will continue next year.

### Reactor Physics, Neutronics and Proliferation

- PEBBED, a fast deterministic two-dimensional neutronic code package suitable for numerous repetitive calculations has been developed. Next year, the code will be extended to 3-D, a state of the art nodal diffusion solver will be implemented and a cross section generation capability will be developed.
- The MCNP4B Benchmark of the HTR-10 has been completed, and VSOP-94 has been implemented.
- The limits of the use of MCNP for pebble bed cores have been established and an MCNP/VSOP linkage has been developed. Next year this link will be improved as well as the core neutronics model of the MPBR. The significance of several approximations such as the double heterogeneity and packing order will be investigated.
- Nonproliferation studies that began this year will continue, including investigation of alternate fuel cycles.

## REFERENCES

1. Scott, Harmon and Holsgraf, "Postirradiation Examination of Capsules P13R and P13S," GA-A13827, October 1976
2. Kovac and Sedlak, "Postirradiation Examination of Capsule GF-4," GA-A160664, October 1980
3. Ketterer et al., "Capsule HRB-15A Postirradiation Examination Report," GA-A16758, July 1984
4. Myers et al., "Capsule R2-K13: Final Report on Cells 2 and 3", HTGR-85-068
5. R. R. Hobbins and R. K. McCardell, "Summary of NP-MHTGR Fuel Failure Evaluations," EGG-NPR-10967, September 1993.
6. F. Ho, "Material Models of Pyrocarbon and Pyrolytic Silicon Carbide," CEGA-002820, Rev. 1, July 1993.
7. G. E. P. Box, W. G. Hunter, and J. S. Hunter, *Statistics for Experimenters*, Wiley, 1978.
8. P. Whitcomb, et al, Design-Expert, Version 3.0, Stat-Ease Incorporated, 2021 E. Hennepin, #191, Minneapolis, MN 55413
9. R. K. McCardell, et al., NP-MHTGR Fuel Development Program Results, Idaho National Engineering Laboratory, 1993, p3
10. J. L. Kaae, et al., "The Mechanical Behavior of Biso-Coated Fuel Particles During Irradiation, Part II: Prediction of Biso Particle Behavior During Irradiation with a Stress Analysis Model," Nucl. Tech., 35, 1977, p368
11. K. Bongartz, et al., "The Brittle Ring Test: A Method for Measuring Strength and Young's Modulus on Coatings of HTR Fuel Particles," J. Nucl. Mat., 62, 1976, p123.
12. Material Specification No. SC-001, Morton Advanced Materials, 185 New Boston Street, Woburn, MA 01801
13. Luigi Massimo, "Physics of High-Temperature Reactors," Pergamon Press, Oxford, England, 1976, pp. 117-125.
14. E. Teuchert, U. Hansen, and K. A. Haas, "V.S.O.P. - Computer Code System for Reactor Physics and Fuel Cycle Simulation," KFA-IRE Report Jül-1649, March 1980.
15. D. R. Vondy and B. A. Worley, "Pebble Bed Reactor Core Physics and Fuel Cycle Analysis," ORNL-5484, Oak Ridge National Laboratory, October 1979.
16. H. Werner, "Build-up of plutonium isotopes in HTR fuel elements - A comparison between computed prediction and chemical analysis," Nucl. Eng. and Design 170 (1997), pp. 147-164.
17. Hans Jung, "Simultanlösung des Abbrand- und Durchlaufproblems der Kugeln bei Kugelhaufenreaktoren" (Simultaneous solution of the burn-up and fuel-movement problems in pebble-bed reactors), Atomkernenergie-Kerntechnik Bd. 38 (1981) Lfg.2, p.141.
18. L. Massimo, "KUGEL, ein Programm, um das raumabhängige Gleichgewicht-Isotopengemisch in einem Kugelhaufenreaktor zu berechnen-Nucleonik" (KUGEL, a program to compute the spatially-dependent neutronics in a pebble-bed reactor with [pebbles of initially] equal isotopic composition), 11Bd., Heft 2, pp.72-76 (1968).
19. Michael G. Izenson, "Effects of Fuel Particle and Reactor Core Design on Modular HTGR Source Terms," Doctoral Dissertation, Massachusetts Institute of Technology, September 1986.
20. Hiroshi Sekimoto, Tohru Obara, Shigeru Yukinori, and Eiichi Suetomi, "New Method to Analyze Equilibrium Cycle of Pebble-Bed Reactors," J. Nucl. Sci. and Tech., 24 [10], pp.765-772 (October 1987).
21. Tohru Obara and Hiroshi Sekimoto, "New Numerical Method for Equilibrium Cycles of High Conversion Pebble Bed Reactors," J. Nucl. Sci. and Tech., 28 [10], pp.947-957 (October 1991).
22. D. Saphier, "DSNP Models Used in the Pebble Bed HTGR Dynamic Simulation", RASG-111-84, Soreq Nuclear Research Center, Israel, April 1984.
23. "Waermeuebergang im Kugelhaufen", KTA 3102.1, KTA, June 1978.
24. M. G. Savage, "A One-Dimensional Modeling of Radial Heat Removal During Depressurized Heatup Transients in Modular Pebble-Bed and Prismatic High Temperature Gas-Cooled Reactors", ORNL/TM-9215, Oak Ridge National Laboratory, July 1984.
25. T. Galen, "Comparison Between Air and Helium for Use as Working Fluid in the Energy Conversion Cycle of the MPBR", S.M. Thesis, MIT, May 2000, Department of Nuclear Engineering.

- 
26. J. Ackeret and C. Keller, "Eine aerodynamische Waermekraftanlage", Schweizerische Bauzeitung, Vol. 113, No. 19, 1939.
  27. C. F. McDonald, "The Nuclear Closed-Cycle gas Turbine (GT-MHR), a Utility Power Plant for the Year 2000", GA-A15184, Nov. 1978.
  28. K. Bammert, "Operating Experiences and Measurements on Turbo Sets of CCGT Cogeneration Plants in Germany", ASME paper 86-GT-101.
  29. Private discussions with Northern Research & Engineering Co., Woburn, MA.
  30. P. Wichner and S. J. Ball, "Potential Damage to Gas-Cooled Graphite Reactors Due to Severe Accidents," ORNL/TM-13661, April 1999.